AN EXPERIMENTAL INVESTIGATION ON AIR POCKET ENTRAPMENTS CAUSED BY SHEAR-FLOW INSTABILITIES IN RAPID-FILLING PIPES

by

Merve Cetin

A thesis submitted to the Graduate Faculty of
Auburn University
in partial fulfillment of the
requirements for the Degree of
Master of Science in Civil Engineering

Auburn, Alabama
December 14, 2019

Keywords: Transition flow in closed conduits, air pocket entrapment, two phase flow, shear flow instability

Approved by

Jose Vasconcelos, Associate Professor of Civil Engineering

Xing Fang, Arthur H. Feagin Chair Professor of Civil Engineering

Frances O'Donnell, Assistant Professor of Civil Engineering

Abstract

Rapid filling conditions in closed conduits, such as the case of sewer filling during intense rain events, can lead to air pocket formation. Such formation creates many operational issues in urban water systems, including the possibility for surging, manhole cover displacement and/or geysering. These problems linked to air pocket formation can cause disruptions in urban areas and results in significant repair costs. To understand flow characteristics under such conditions, an experimental research on air pocket entrapment mechanism based on shear flow instabilities (SFI) was developed. A fully filled horizontal water pipe was opened at the downstream end to create a cavity flow and air intrusion of varying thickness. After some time, a second valve was maneuvered near the upstream end triggering inflow admission and flow pressurization. The inflow front pushed air in high velocity over the free surface, and in some cases, air pocket entrapment was observed. Existing threshold criteria for SFI have been assessed with the experimental observations of pocket formation. Also, velocity for pressurized front and air intrusion, and pressure values during the experimental runs have been measured. This study sheds more light on the issues and associated risk of air pocket entrapment in existing water systems.

ACKNOWLEDGEMENTS

I would like to thank General Directorate of State Hydraulic Works (DSI) under Republic of Turkey Ministry of Forestry and Water Affairs for financial support which has provided for me with the grant number of 33070922-772.02-826712 supporting my studies in the USA.

I would like to express my warmest gratitude to my kind academic advisor Dr. Jose Vasconcelos for his supportive, understanding, and patient guidance. I will always be grateful for all his support and encouragement. He continually guided me through all the hard time of my research. His patience is appreciable. I wholeheartedly thank Dr. Xing Fang, and Dr. Frances O'Donnell for agreeing to be my committee member and review my thesis and providing me their kind guidance. Last but not the least, I would like to thank Auburn University for providing the chance to do my research.

I am grateful to my mother Ayşe Çetin and my father Erhan Çetin. Thank you for your compassion, continuous support, helping me believe that nothing is more precious and important than me and believing in me more than I do myself. To my wonderful and precious treasure; my sister Büşra Çetin and my brother M. Sefa Çetin, thank you for your support and unconditional love. I love you all so much!

TABLE OF CONTENTS

LIST OF TABLES

LIST OF FIGURES

LIST OF ABBREVIATIONS

A_{pipe} Pipe cross sectional area = $\pi * D^2 / 4$

A_{fs} Free surface area

A_{cavity} Cross sectional area of the cavity

C_{air} Celerity of the air cavity

D Pipe diameter

D_C Gap between the weir crest and the pipe crown at the downstream end

D_C^* Normalized gap between the weir crest and the pipe crown at the downstream end = D_C/D

f Friction factor

F_I Interfacial Froude number

Fc Critical Froude number

H_R Water level at the upstream reservoir

H_R* Normalized upstream reservoir head ($H_R* = H_R / D$)

h_{water} Hydraulic depth of water

h_{air} Hydraulic depth of air

K Local loss coefficient at pipe connection with upstream reservoir

Kf Correction factor

Lc Length of the rigid column

Q Flow rate in the pressurized flow calculated using the rigid column model

SFI Shear flow instability

t Time

V_a Air velocity

V^* Normalized velocity (V^*=Velocity / $(g*D)^{0.5}$)

V_{fs} Velocity of water in free surface regime

V_{water} Velocity of water

Y_{dw} Water level at the downstream end of the pipe

λ Wavelength of the water wave

μ Dynamic viscosity

ρ Density

ρ_{water} Density of water

ρ_{air} Density of air

Chapter 1. Introduction

Rapid filling of closed conduits is characterized by the uncontrolled water inflow admission into closed conduits such as storm water sewers and tunnels. During fast filling in closed ducts, air pocket entrapment may occur in the duct leading to adverse air-water interactions. These interactions include air-water surging and structural damage (Zhou et al. 2002), stormwater geysering (Muller et al. 2017), manhole cover displacement (Jue and Vasconcelos 2017), among other operational issues. In addition to rapid filling in stormwater system, air pocket entrapment can occur in other infrastructure such as drinking water transmission pipelines, irrigation systems and other essential infrastructure. Such air-water interactions can cause big disruptions in our daily lives and serious repair costs.

Although these air pocket entrapment mechanisms may cause such important problems, this issue is still not fully understood. Some investigations have addressed air pocket entrapment indirectly, associated with specific rapid-filling inflows (Haman and McCorquodale 1982; Zhou et al. 2002; Arai and Yamamoto 2003). This study aims to provide further insights on the air pocket entrapment mechanism that may be generated by shear flow instabilities (SFI), which is one of various air pocket entrapment mechanisms. Air pocket characteristics and behavior in the rapid filling conditions were systematically investigated through experimental tests.

SFI is a type of Kevin-Helmholtz instability that occur in closed conduits when depth nears the pipe diameter and there are high relative velocities between air and water phases. SFI may

occur when pipe filling bores move at high velocities pushing the air phase in the pipe in the direction of flow and generating water waves. When these water waves touch the crown of the pipe at both their ends, air pockets are formed, as described in Li and McCorquodale (1999). Studies that have presented a threshold for SFI occurrence include Li and McCorquodale (1999) and Kordyban (1990). In this study, the accuracy these threshold criteria were examined and a lumped-inertia flow model was also developed.

The present study has its limitations in that the experimental apparatus did not enable the measurement of the air pocket thickness and volume. This limitation impacts some of the analysis presented, but through using CFD results associated with these tests this was overcome. Nevertheless, this investigation makes use of an innovative experimental apparatus, and provide a dataset that will be useful in the context of air-water interactions in closed conduit flows.

Chapter 2. Literature Review

2.1 Horizontal Motion of Entrapped Air and Operational Issues Associated with Rapid Filling in closed conduits systems

Various operational problems can be occurred when exposed to rapid flow conditions associated with intense rain events in closed channel systems like storm water systems. These problems can be given as examples of excessive surging, overflows, large pressures, and manhole lid displacements, among others, (Muller et al. 2017). In such conditions, there are negative impacts to the environment and public health, as well costs associated with related structural damage. The flow characteristics including velocity, pressure, and overall compressibility are affected if there is air in the system, (Vasconcelos and Wright 2011). Air phase has different aspects and formats in closed conduits within urban water systems. The air phase present in urban water systems can be categorized either as small bubbles or larger air pockets. When small air bubbles enter into the system, they may collect at high points along with an undulating and can combine to form larger air pockets, (Ramezani et al. 2016). This process is defined as air entrainment (Chanson 1996). Otherwise, when large amounts of air are captured, this is referred to as air pocket entrapment, which is the focus of the present work.

When inflow rates are gradual, pressurization interfaces are nearly horizontal and air pocket formation is not observed (Patrick and Vasconcelos 2015). However, when in case of rapid filling, various air pocket formation mechanisms can take place, as presented in prior experimental

investigations (Li and McCorquodale 1999; Vasconcelos and Wright 2006). Entrapped air pockets have been linked to various operational problems in storm water systems, including surging, structural damage, manhole cover displacement, and geysering events (Muller et al. 2017). Many of these problems are created either by the compression of air phase or by uncontrolled air release from pressurized systems.

Once entrapped, air pockets can move within tunnel systems as discrete gravity currents, as described by Baines (1991). The pocket celerity depends on various factors, such as air pocket volumes, shear stress, and background flows etc. Figure 2.1 shows the background flows and shear stress affected a backward-moving air pocket motion in a horizontal slope pipe (Chosie et al. 2014). Also, when air pockets arrive at the base of a water filled ventilation shaft, these pockets move vertically displacing water and possibly leading to geysers (Vasconcelos and Wright 2011; Lewis and Wright 2012), as illustrated in Figure 2.2.

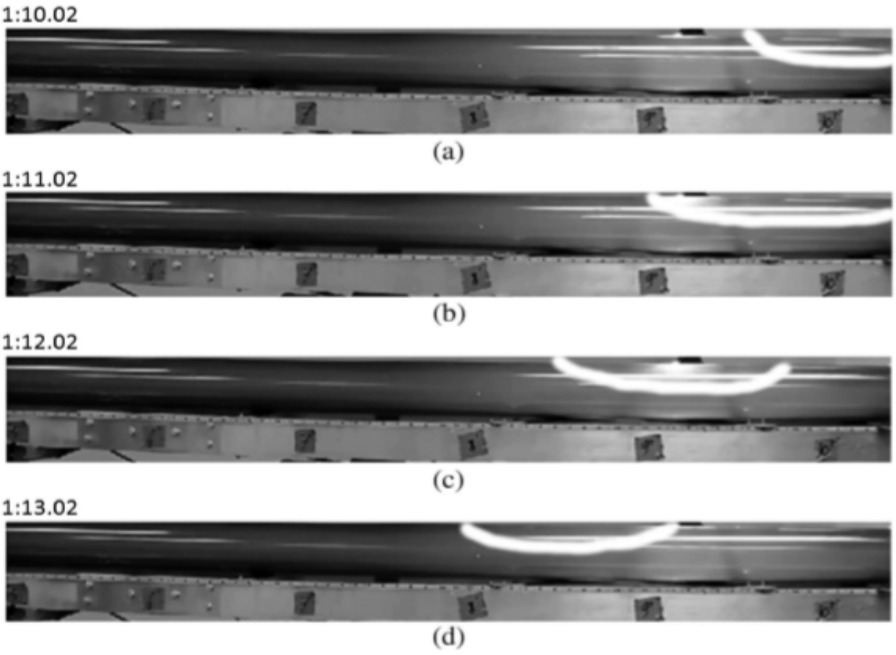

Figure 2.1: Snapshots of air pocket moving in a horizontal pipe (Chosie et al. 2014)

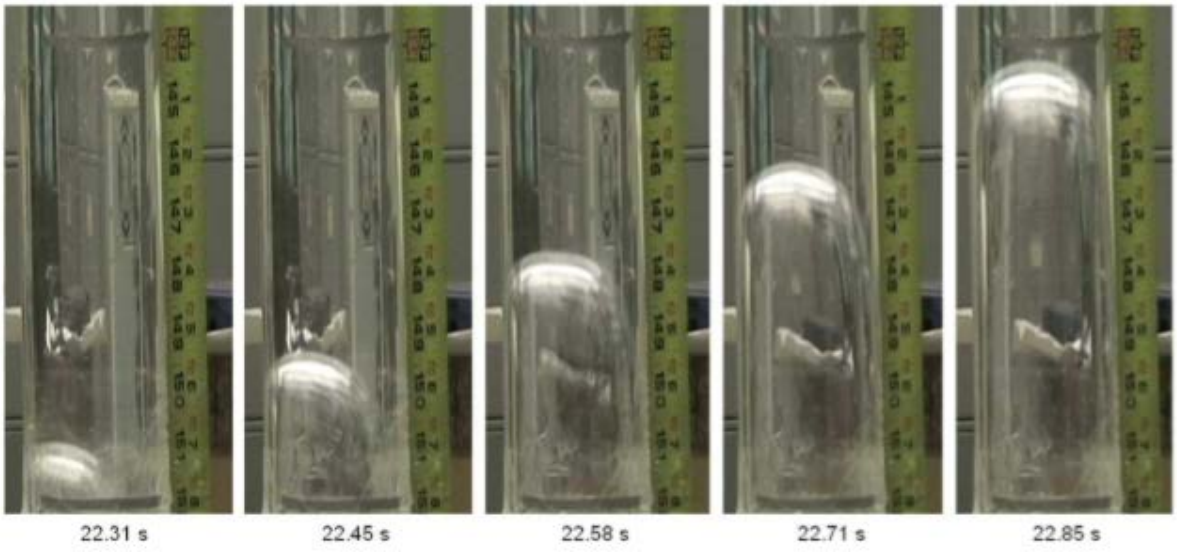

Figure 2.2: Rising motion of air pocket in a vertical pipe (Vasconcelos and Wright 2011).

One of the worst impacts of air pocket entrapment is the structural damage that is linked to air-water surging. The pioneer study by Martin (1976), which was followed by Zhou et al. (2002) among others, showed that compressed air pressure can greatly exceed the pressure that drives the flow prior to air compression, as displayed in Figure 2.3. The worst impact of air pocket entrapment is the structural damage that leads to increased surging. It was caused by compressibility of air in systems, leading to significant pressure surges, which in turn create forces that may exceed design assumptions.

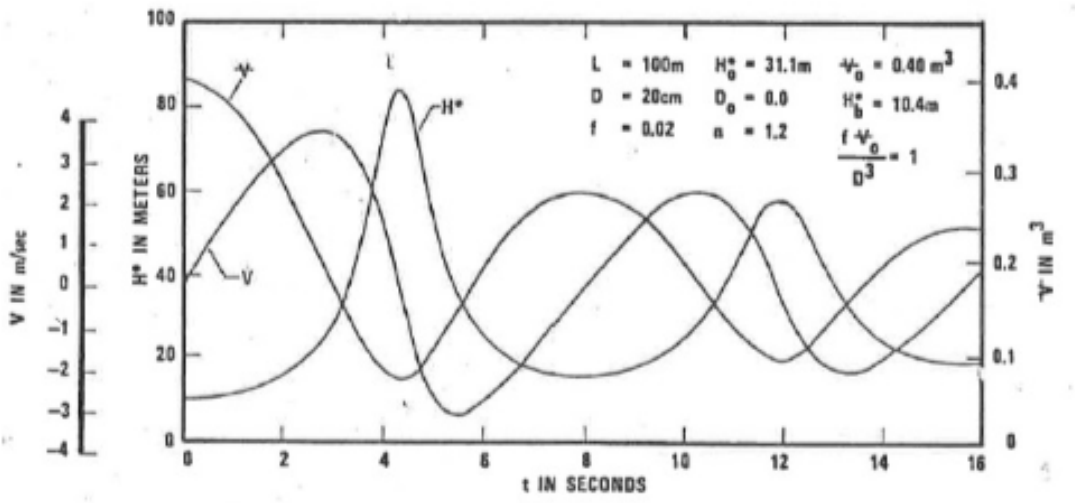

Figure 2.3: Transient air pressure, liquid velocity and air volume during air-water compression in a closed pipe (Martin 1976).

Zhou et al. (2002) pointed out that such compression may be behind an episode in which an entire manhole structure was blown off the pipe in Edmonton, Alberta. This study also categorizes pressure oscillations model in to three types of behavior: Type 1 - Negligible Water Hammer Effect, Type 2 - Mitigated Water Hammer Effect, and Type 3 - Water Hammer Dominated. These types were grouped by observing the pressure oscillations related to changing the size of the ventilation orifice located at the downstream end of the experimental apparatus. Figure 2.4 shows the pressure peaks related to the most extreme of these behaviors, Type 3, which created a great potential for structural damage.

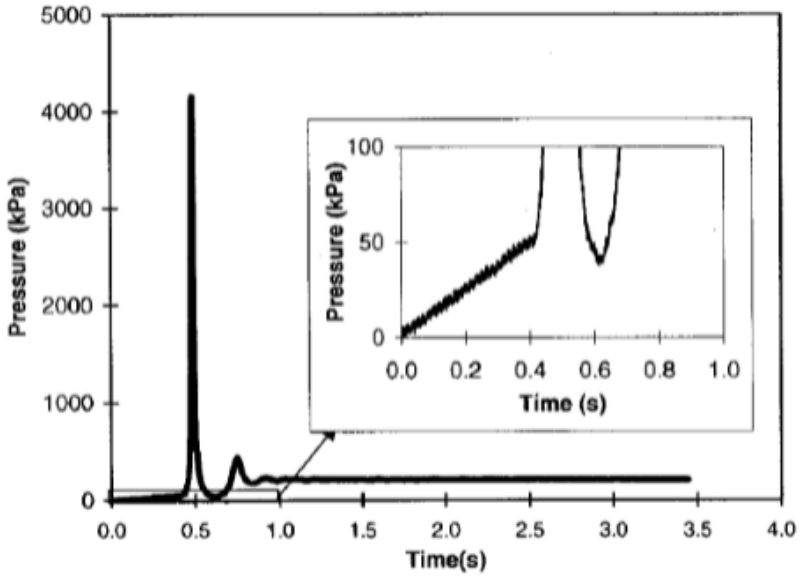

Figure 2.4 : Pressure oscillation pattern for water hammer effect (Zhou et al 2002).

2.2 Studies on gravity currents

An associated field of investigation involving air-water flow in closed conduits is the propagation of gravity currents, particularly the case of non-Boussinesq currents such as the intrusion of an air cavity in a pipe initially filled with water without air. Classical contributions in fluid mechanics in this area are exemplified in the works by Benjamin (1968), Wilkinson (1982), Baines (1991), and Simpson (1997) among others. Such air cavities are referred to as gravity currents in this context.

These studies in gravity currents are not directly linked to air pocket entrapment, however, in the context of the present research, gravity currents allow for the creation of air layers of uniform thickness in the pipe. Thus, the initial stages of the experimental tests involved the creation of a gravity currents, which was followed by a rapid filling pipe process. The discussion that follows only intends to provide a brief overview of the characteristics of gravity currents flow.

Benjamin (1968) studied gravity currents that advanced throughout the upper boundary of a liquid referred to as air cavity. In present study benefit from the Benjamin's air cavity approach pretty much. The author derived an equation for the maximum velocity of an advancing air pocket when water is discharged from the end of the horizontal pipe. He also proposed an argument that thickness of an advancing air pocket could not be more than half of the pipe diameter without the motion is stopped. These findings are useful for general design and for the prediction of air-pocket behavior, but the pocket celerity depends on various factors, such as air pocket volumes, existence of background flows, opposition between buoyancy and drag forces, etc. (Chosie et al. 2014).

The work by Benjamin (1968) was pioneer in establishing that the air cavity celerity scales with $\sqrt{gH}$, with g H the conduit characteristic dimension (i.e. diameter). Among various important observations, it was found that the gravity current celerity generally decreased with its thickness. Also, Benjamin (1968) differentiated the dissipation-free (energy loss-free) intrusion and the dissipative air cavity intrusion (e.g. having a trailing hydraulic bore, shown in Figure 2.5).

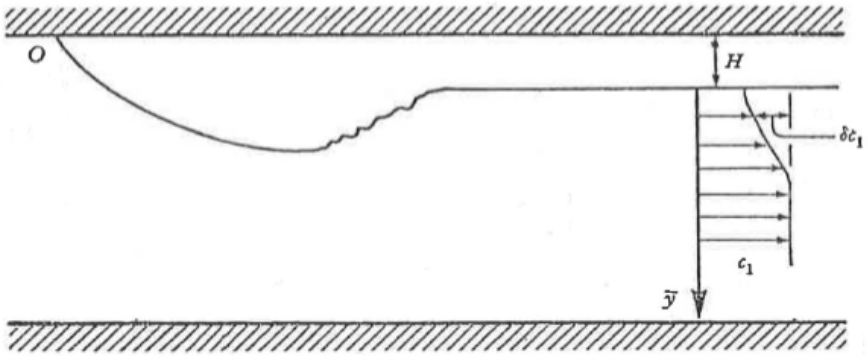

Figure 2.5: Gravity current propagation velocity adapted from Benjamin (1968).

According to Benjamin's steady-state assumption, the celerity of the cavity in a fully open horizontal circular pipe is $0.542(gD)^{1/2}$. At the stagnation point O, the pressure was admitted as zero through the free surface. Townson (1991) presented results that indicate that when circular pipe geometry is considered the cavity speed did not change substantially, as indicated in Figure 2.6. In the graphs, U_0 corresponds to the term C_1 in Equation 2.1, D_1 is the pipe diameter D, D_2 is the free surface flow thickness h. The terms E_J, E_C and $E_S$correspond to energy loss for dissipative cavity motion conditions.

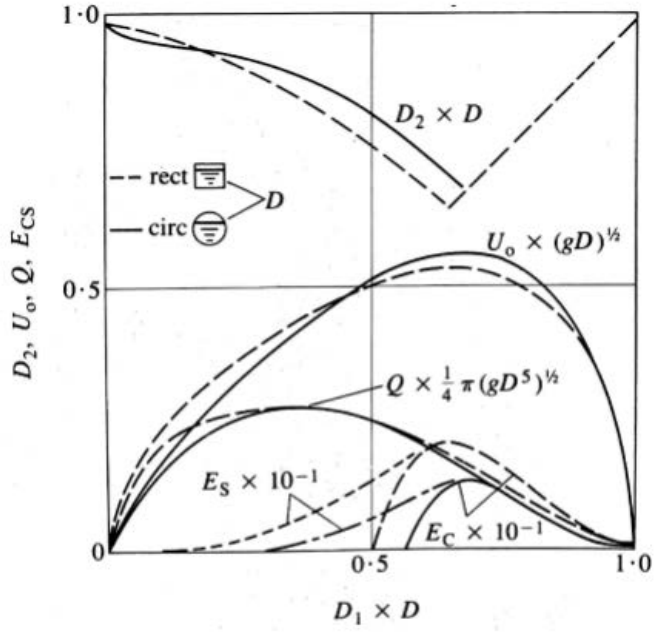

Figure 2.6: Characteristics of gravity current motion of circular and rectangular pipes presented by Townson (1991).

The experimental investigation on the movement of large long air bubbles in stationary water in a horizontal channel of rectangular cross-section by Gardner et al. (1970) confirmed the results by Benjamin (1968) for very deep channels. This investigation also focused on the explanation of the influence of surface tension on bubble velocity. Furthermore, in this study, the

bubble velocity is constant with respect to the distance and is similar to that designed by Benjamin (1968), with the exception of the tip of the curved nose front near the top wall of the channel. A limitation of these studies is the lack of ambient water flow.

Wilkinson (1982) combined surface tension effects that have significant impacts on the shape and celerity of the air cavity, improving the description for the propagation of air cavities of smaller thickness. In that study, control volumes were used to understand better frontal region and bore region of the cavity to be treated as steady flows. It may be unsteady, although the flow is related to the admission of air into a long duct.

Baines (1991) studied the gulping phenomenon of air, leading to discrete air pocket entrapment in a horizontal pipe . This entrapment occurred in horizontal pipes with a crest or partial opening at the outlet. Motion of such pockets was defined in Baines (1991) shows similarity with continuous air cavities such as the ones studied by Benjamin (1968). This work showed that the observed celerity increased slightly with the tested slopes (up to 8 degrees), as seen in Figure 2.7, and that celerity values of discrete air pockets scaled with $\sqrt{gD}$.

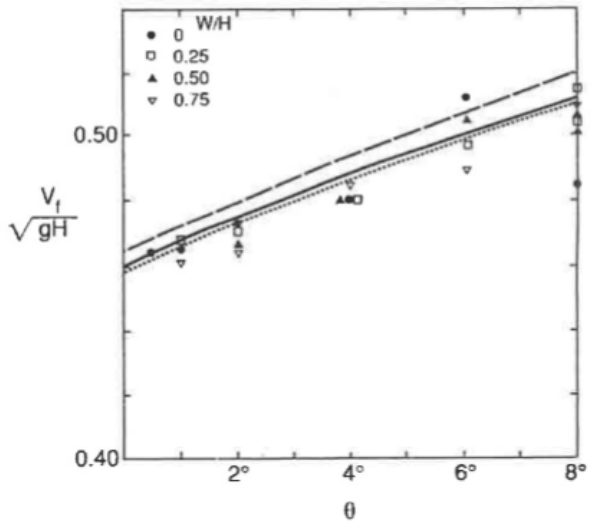

Figure 2.7: Velocity as function of channel slope from Baines (1991).

Simpson (1997) discussed on finite-volume cavities, including experimental studies in which a fixed volume of air into a closed horizontal tank full of water. These experiments associated with development of a gravity current of air that is released from behind a gate as it advances above the water, as shown in Figure 2.8. In the initial phase, the pocket front occupying almost half the depth of the tank, and the pocket is moving at a constant speed. In the intermediate phase a hydraulic bore formed at the tail of the gravity current, and at the last phase this bore has reached the head of the gravity current, and the speed during this phase is no longer constant.

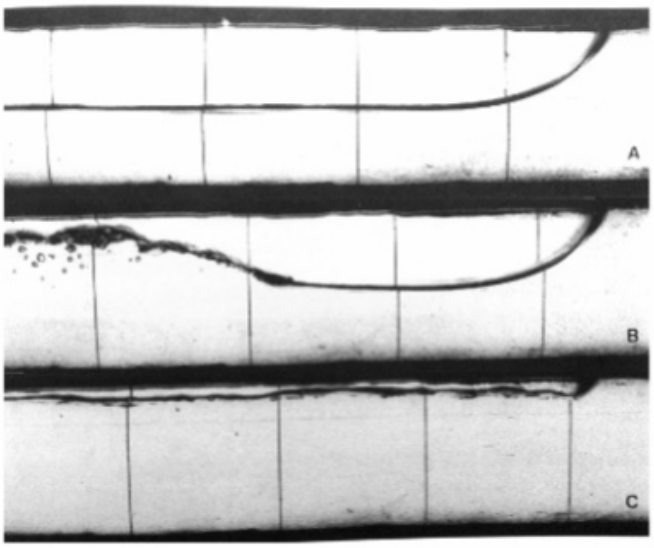

Figure 2.8: Three phases of advancing air volume released from one end of a channel of water (Simpson, 1997)

Vasconcelos and Wright (2008) presented an experimental and numerical work on the advance of an air cavity considering the acceleration of the water column due to varying pressure gradients. Figure 2.9 displays the advance of air intrusion observed in experimental work

compared to the authors' numerical prediction. The initial advance of the air cavity is gradually stopped and returned by the water column velocity. For the smallest values of H/D (pressure head at the reservoir divided by the pipeline diameter), observed and predicted trajectory agree well, but for increasing values of H/D the results were not as accurate.

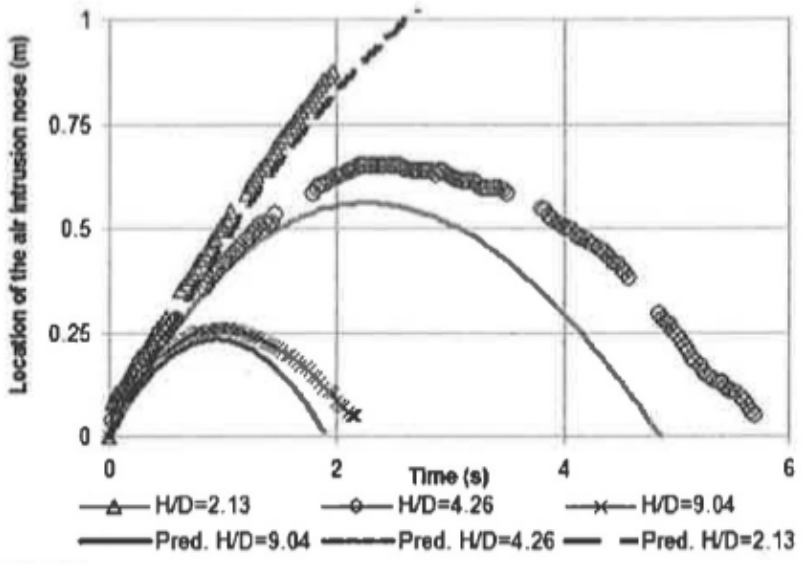

Figure 2.9: Comparison of advance of air intrusion observed in experiments with numerical prediction by Vasconcelos and Wright (2008).

2.3 Entrainment and entrapment of air pockets in closed conduits

Many reasons can lead to the air entrainment in transmission mains have been presented to date, and a comprehensive summary is presented by Lauchlan et al. (2005). These mechanisms include 1) entrainment at inflow at drop chambers, inlet, or intake and outflow; 2) entrainment due to vortices, turbulence and hydraulic jumps; 3) insufficient pump submergence; 4) filling or emptying of pipelines; and 5) negative pressures at the pipe inlet. Particularly in the context of stormwater systems, air entrainment is very relevant in manholes and dropshafts with flow

plunging processes, (Rajaratnam et al. 1997); (Gualtieri and Chanson 2013). Air can be entrained into dropshafts in a few ways, (Rajaratnam et al. 1997); (Granata et al. 2014); (Gualtieri and Chanson 2013): (1) entrainment by the inflow impingement to the vertical shaft wall, (2) air dragged by the falling water streams and drops in the dropshaft, (3) entrainment by the flow plunging into the bottom pool, and (4) entrainment by theturbulent outflow. For tall dropshafts, the water breaks up into water drops and its effect on air entrainment can be significant is the expected, (Ma et al. 2016).

Albeit relevant, these mechanisms are not focused in the present research. Figure 2.10 illustrates Water flow inside the dropshafts in different patterns.

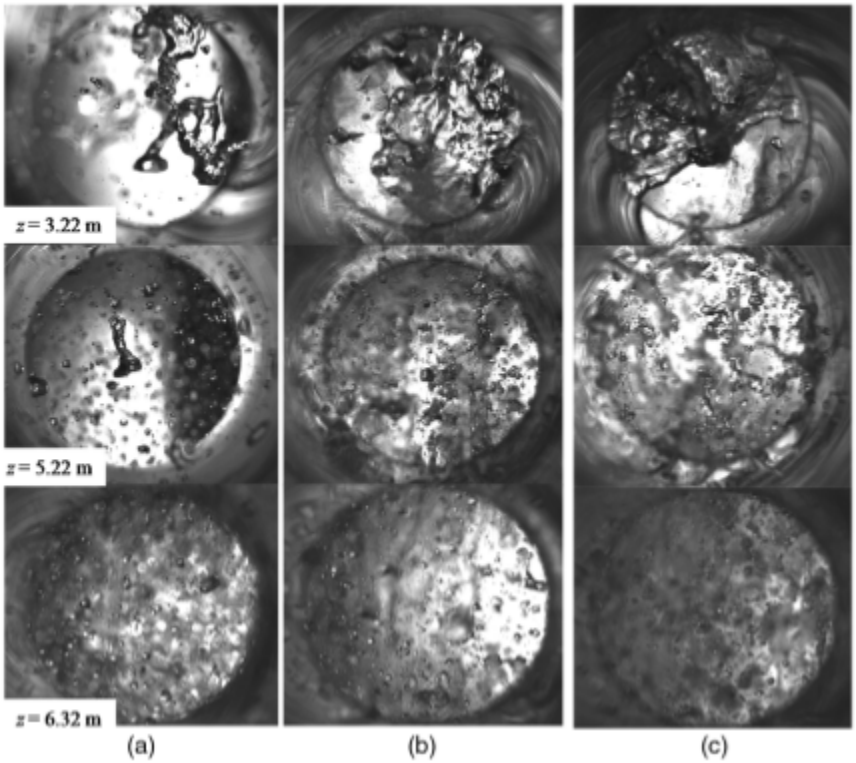

Figure 2.10: Water flow inside the dropshafts at s= 10 cm under (a) Qw = 3.9 L/s; (b) = 18.6 L/s; (c) =33.5 L/s; the water flow direction in the photos is from top to the bottom (Ma et al. 2016).

By comparison, research on air pocket entrapment has been more recent and limited. According to (Hamam and McCorquodale 1982), relative motion between air and water can lead to surface waves in water which lead to interface stability. Eventually this interface stability caused to form an air pocket entrapment. This and other mechanisms for air pocket entrapment in the context of storm water systems have been studied experimentally by (Vasconcelos and Wright 2006), which also includes mechanisms such as insufficient or misplaced ventilation (Figure 2.11), breakdown of pressurization air-water interfaces (Figure 2.12), interface breakdown mechanism (Figure 2.13), and gradual flow regime transition (GRFT) as shown in Figure 2.14.

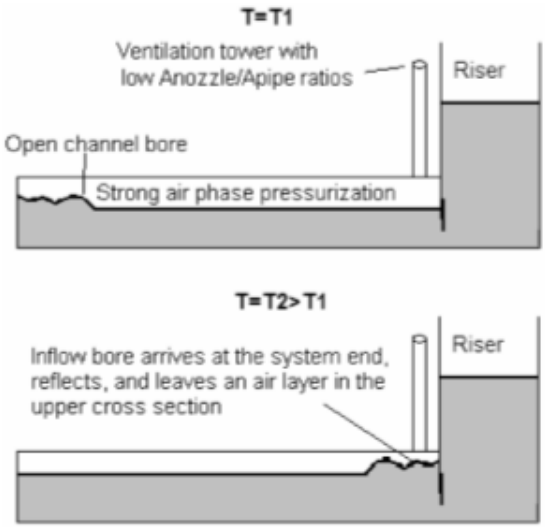

Figure 2.11: Inadequate ventilation mechanism for air pocket entrapment (Vasconcelos and Wright 2006)

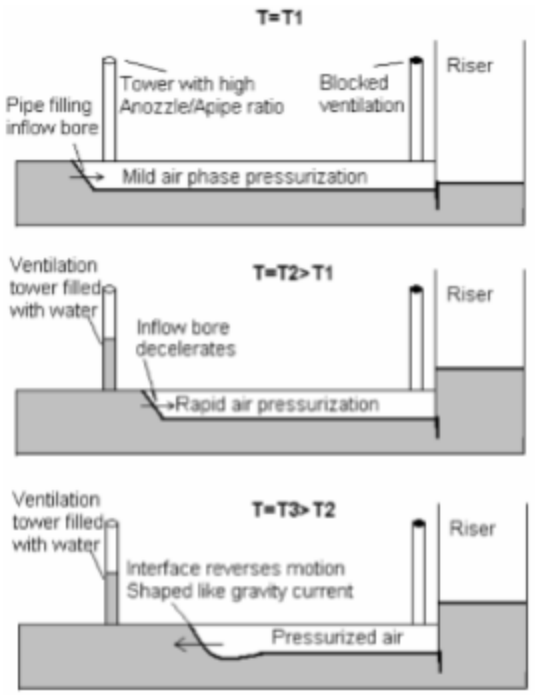

Figure 2.12: Breakdown of pressurization air-water interfaces for air pocket entrapment

(Vasconcelos and Wright, 2006)

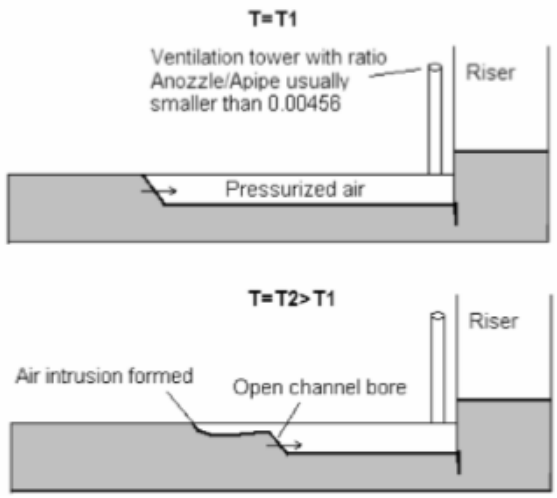

Figure 2.13: Interface breakdown mechanism for air pocket entrapment (Vasconcelos and Wright 2006)

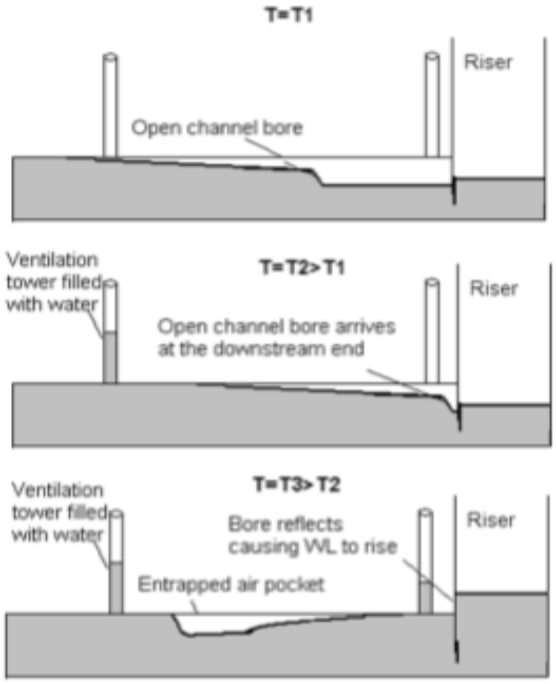

Figure 2.14: Gradual flow regime transition (GRFT) mechanism for air pocket entrapment (Vasconcelos and Wright 2006)

In Figure 2.15 an air pocket formation mechanism is illustrated within a numerical simulation of rapid filling scenario. Here, as a reaction of an inflow front from the system boundary, a large air pocket was entrapped. This is an undesirable situation and can only be evaluated if this pocket is discharge through a water-filled ventilation pipe for kinematic of air pocket mechanism.

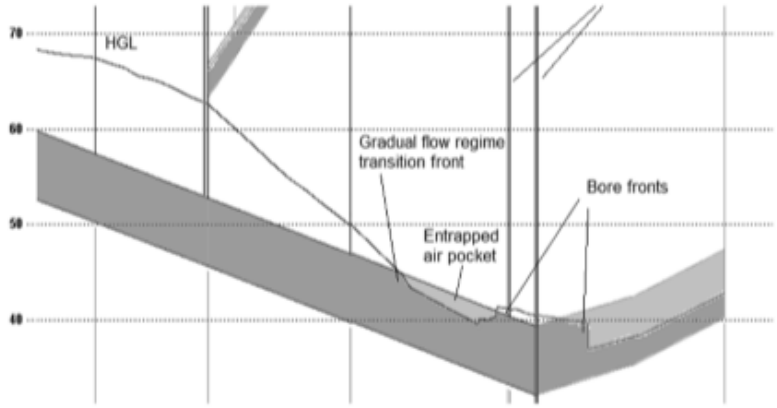

Figure 2.15: The reflection of inflow fronts from the system boundary caused air pocket entrapment (Vasconcelos and Leite, 2012).

More studies related to the formation and motion of air in stormwater systems are illustrated by Li and McCorquodale (1999), Zhou et al. (2002) and Lautenbach et al. (2008). A mathematical framework for the simulation of flow regime transition (also referred to as mixed flows) using lumped inertia analysis and the ideal gas law, and consider the mechanism for air pocket formation based on shear flow instabilities was presented in the study by Li and McCorquodale (1999). In the formulation the location of the air-water interface is calculated explicitly, providing then means to compute the advance of an entrapped pocket. Nevertheless, the velocity of the air bubble, instead of calculated by the model, uses as a calibration parameter in the simulations

Air trapped in a rapidly filling pipe can induce high-pressure surges, especially when air leakage occurs. The air leakage could occur through the manholes in a sewage system, which causes the manhole cap displacement or geysers (Zhou et al. 2002). The pressure peaks observed from the experiment are certainly high enough to blow off manhole covers and explain sewer rupture. The pressure in some cases rises to two or three times of the acting pressure at the

upstream. According to Zhou et al. (2002), the pressure is at least one order of magnitude greater than the structural loads for which typical urban sewer systems are designed.

Below-grade stormwater storage tunnels are an increasingly popular method of capture excess runoff and control combined sewer overflow events. As tunnels fill, it is important to consider the potential effects of transient surges, including high hydraulic grade lines, geysering caused by trapped air, and the force of rapidly moving bores on tunnel infrastructure (Lautenbach et al. 2008). Some numerical models are developed to find the possible locations in the Tunnels system where the air could be entrapped. These models are used to simulate transient surges as part of the evaluation of the proposed tunnel geometry, as it was the case of a large tunnel system associated with the Long Term Control Plan to reduce flooding and CSOs in sections of District of Columbia stormwater drainage system (Lautenbach et al. 2008) .

2.4 Shear Flow Instabilities

Shear flow instability (SFI), is the main focus of this work. These are a type of Kevin-Helmholtz instability, with the characteristic that they occur in closed conduits, and as result they accelerate the development of pressurized flow conditions and appearance of entrapped air pockets. The Kelvin–Helmholtz instability can occur when there is velocity shear in a single continuous fluid, or where there is a velocity difference across the interface between two fluids (Batchelor 1967). An example is wind blowing over water: the instability manifests in waves on the water surface. The Kelvin-Helmholtz instability caused by a turbulence of two air layers lying close to each other, which move with different speed and/or direction.

Kelvin Helmholtz instability was explained by Batchelor (1967) in its physical mechanism in terms of vorticity dynamics. The local strength of the sheet is presented by the thickness of the sheet,

shown in Figure 2.16. The arrows show the directions of the self-induced movement of the vorticity in the sheet, and show (a) the accumulation of vorticity at points like A and (b) the general rotation about points like A, which together lead to exponential growth of the disturbance.

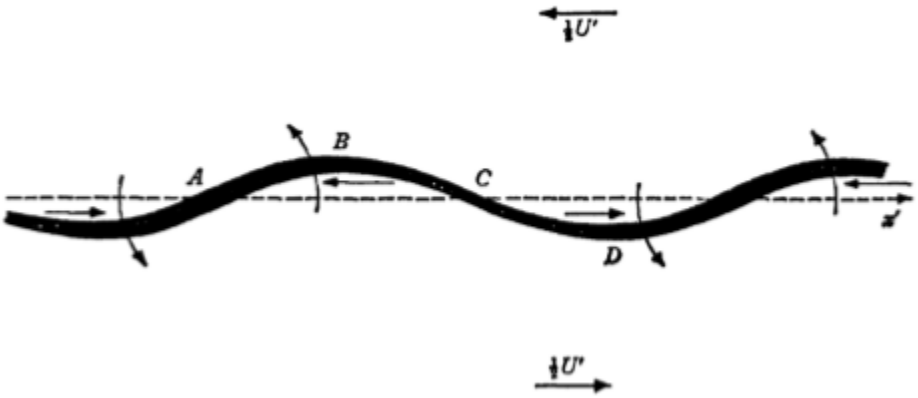

Figure 2.16: Growth of a sinusoidal disturbance of a vortex sheet with positive vorticity normal to the paper (Batchelor 1967).

SFI is defined by Hamam and McCorquodale (1982) as the interfacial disturbance that lead to the formation of air pockets on the surface, analogous to Kevin Helmholtz instabilities. Baines and Mitsudera (1994) observed SFI occurrence in cases when air-water flows were the opposite direction with comparable velocity. Figure 2.17 illustrates air pocket formation mechanism caused by SFI that (Vasconcelos and Wright 2006) presented.

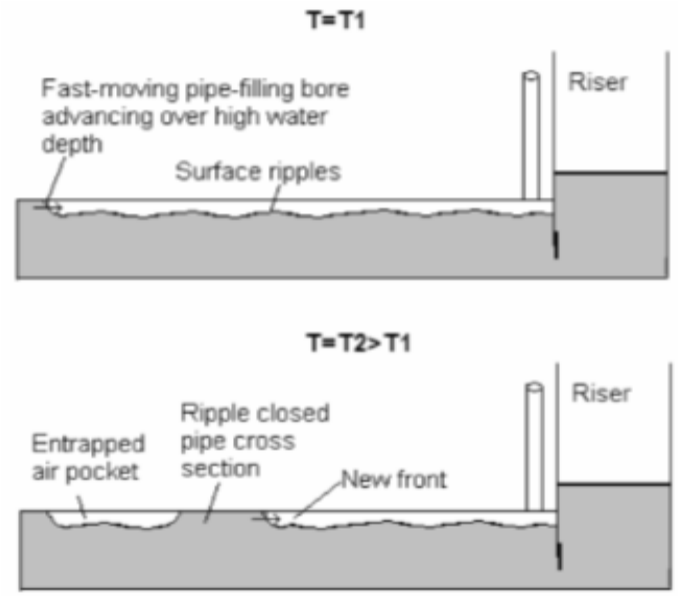

Figure 2.17 : Air pocket entrapment due to shear flow instability (Vasconcelos and Wright 2006).

Kordyban (1990) developed a criterion for the formation of SFI in closed pipes, which depend on the relative flow velocity and fluid densities within the pipe. An alternative threshold criteria for SFI was presented in Li and McCorquodale (1999). The authors studied the development of SFI during rapid filling of conduits in investigations that include experiments. According to the authors, SFI occurrence depended on, flow velocity, flow height, entrance and discharge condition, pipe characteristics (diameter, length), and wave height. A schematic of the transition flow from free surface flow to pressurized flow reported by the Li and McCorquodale (1999) is shown in Figure 2.18.

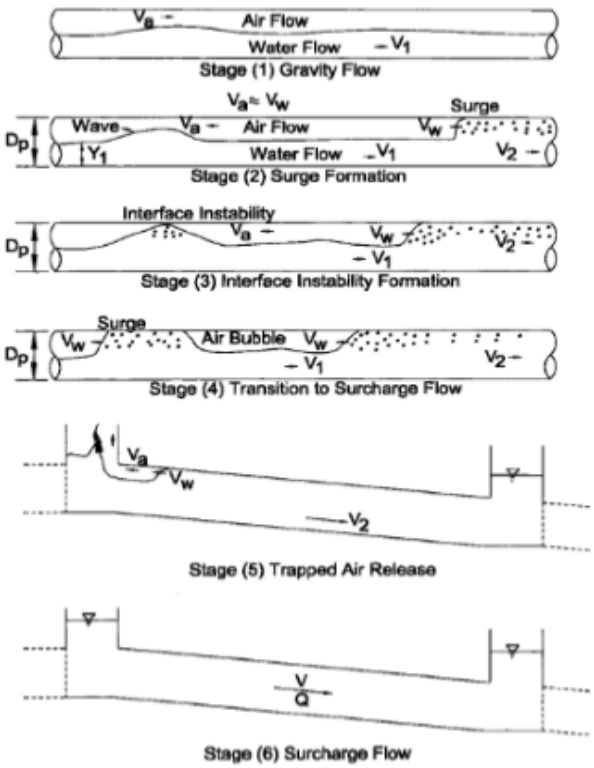

Figure 2.18 : Steps in transition of free surface to pressurized flow (Li and McCorquodale 1999)

In summary, it has been acknowledged that air pocket entrapment creates operational problems in stormwater systems and similar closed duct systems. These problems are relevant, however the absence of any systematic experimental studies on SFI as an air pocket formation mechanism is an important knowledge gap. This motivated the present study, as is further detailed in the Objectives chapter.

Chapter 3. Objectives

The purpose of present work is to study the SFI mechanism for air pocket formation during rapid filling episodes in closed conduits through a systematic experimental program. Ultimately, the goal is to gain further insights on these events and help advance research on air-water interactions in closed conduits. The work has the following specific objectives:

• Understand cases of rapid filling in which pipe-filling bores would characterize the filling process, and contract with cases in which air pockets appear

• To research and identify the physical conditions (by changing weir height at the discharge point and changing pressure head at upstream) that lead to pocket formation caused SFI (shear flow instabilities)

• To compare existing SFI threshold criteria with experimental observations of these events.

Chapter 4. Methodology

4.1 Experimental Apparatus

The experimental apparatus used in experiments was installed on a horizontal slope, as represented in Figure 4.1 sketch. The apparatus included a 9.8m long clear PVC pipeline, which include three 3.05-m long clear PVC pipes with diameter *D* equal to 0.102-m. The pipes are connected to each other through rubber joints tightened with a screw-adjustable metal clamp. Other junctions in the apparatus were sealed with caulk. A reservoir was connected to the pipeline at the upstream end through a 102-mm knife gate valve that is hereon referred to as upstream valve. This reservoir capacity was 0.29 m3 it was filled with water with varying heads above the pipe invert.

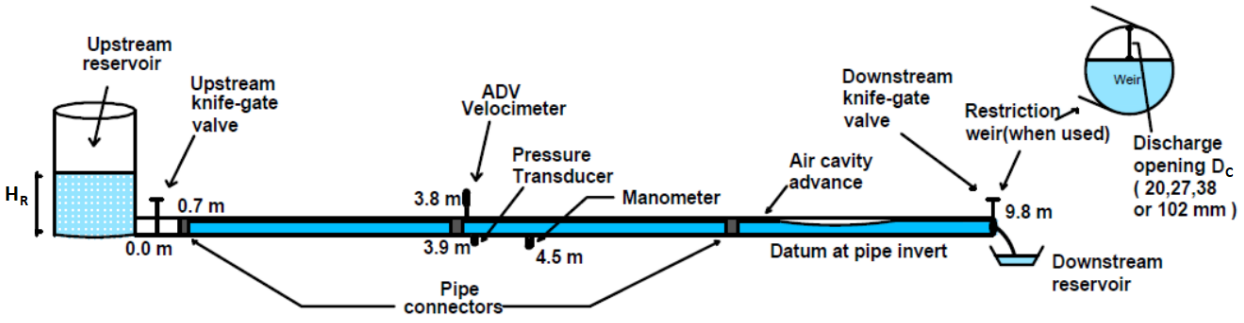

Figure 4.1: Sketch of the system of and the experimental apparatus.

With the upstream valve, the supply reservoir was separated from the pipeline and the opening enabled rapid filling conditions and pressurization in the pipe. There was also a second

102-mm knife gate valve at downstream end of the apparatus, hereon referred to as downstream valve. Through the opening of the downstream valve, water discharge out of the pipe initiated, allowing for the admission of an air cavity that advanced in the horizontal pipeline. The positioning of optional weirs at the downstream end of the apparatus, after the downstream valve, enabled that the advancing air cavity had different thickness values. As is further explained, after the cavity advanced in the apparatus, the upstream valve was opened and initiated the rapid filling conditions. In all, four different downstream water discharge conditions existed with the use of free discharge and three weirs that left different gaps between the pipe crown and the edge of the weir.

In order to characterize of movement of the air cavities, pipe-filling bores, air pockets and perform related flow measurements during the tests, the following instruments were used:

- Head measurement: A manometer (EXTECH HD750) measured pressure heads (up to 3.5 m) at the initial and final stages of the experiment, 4.5 m away from the upstream end.
- Velocity measurements: A NORTEK Vectrino ADV was installed 3.8 m away from the upstream end of the pipe to record the velocity, installed in the pipe centerline. It sampled water velocity at a location 20 mm away from the invert. The accuracy of measurements was 0.5% or 1 mm/s (whichever was higher), and frequency of data collection was 25 Hz.
- Data acquisition: A National Instrument NI-USB 6210 board was used in the acquisition of pressure data.
- Three digital HD camcorders: recorded the overall experiment at 1080p resolution, 30 frames per second, and recorded flow profiles within each of the three clear PVC pipes.
- Pressure measurements: One piezo-resistive pressure transducer (Model MEGGIT ENDEVCO 8510C-50) was used to record the pressure during the experiment at the pipe invert, 3.9 m away

from the upstream end. The sensor can measure pressures heads up to 35 m, with an accuracy of 0.01 m, and sampled at a frequency of 200 Hz.

4.2 Experimental Procedure

A description of the experimental run is as follows. Varying experiment variables included the three different reservoir heights and four different downstream discharge conditions obtained with the full discharge conditions or with the sharp-crested weirs. A combination of the three reservoir levels and four different downstream weir opening values yielded a total of 12 experimental conditions. Each of these conditions were repeated at least 3 times to ensure consistency of experimental measurements. The reservoir was filled with water with varying heads H_R of 0.305 m, 0.610 m and 0.915 m above the pipe invert. Immediately after the downstream valve, different restriction weirs were optionally installed to limit water discharge. These sharp-edged weirs were placed along the cross section of the pipe endpoint. Each weir yielded a different gap (referred to as D_C) measured between the weir crest and the pipe crown, and the size of the gaps created by the weirs were 20 mm, 27 mm, 38 mm. The weir geometries were selected after preliminary testing with the apparatus and aimed to create a range of flow conditions that yielded SFI. When no weir was present (i.e. full discharge conditions), it was considered that D_C^* (defined as D_C/D) was equal to the pipe diameter.

The first step in the experimental runs was to set the downstream flow conditions by either using a fully open condition (i.e. no weir) or selecting one of the restriction weir sizes for the partially opened cases. The field of recording of the cameras was adjusted to capture the entire horizontal pipeline length. The horizontal pipe was filled with water, and all the air bubbles were swept away from the pipe. Even a small air bubble was pulled out of the pipe and the pipe was completely airless, filled only with water, and set in quiescent conditions prior to the opening of

the valves. The reservoir at the upstream was then filled with water at the pre-determined height, either 0.305 m, 0.610 m or 0.915 m.

The instruments were then initiated with the start of the three HD camcorders, and the experiment conditions were reported to the cameras. Piezo-resistive transducer and velocity-meter ADV were started. The initial pressure was read and recorded from the manometer. The knife gate valve at the downstream end was opened quickly (less than 0.5 second), and an air cavity propagated upstream near the pipe crown. A schematic of air cavity shows in Figure 4.2 with a sketch. When air cavity advanced within 1.8 to 2.5 meters from the upstream reservoir, the upstream valve near was quickly opened. This quick opening of the upstream knife valve is started the rapid filling process and caused form a pressurized bore interface. A schematic of the pressurized bore shows in Figure 4.3 with a sketch. Depending on the experimental conditions, the rapid flows would be characterized by the advance of the pipe-filling bore all the way until the downstream end or alternatively by air pocket formations due to SFI. Inflows were admitted into the upstream reservoir during this inflow to reduced reservoir water level during the rapid filling stage, thus inflows were admitted to the reservoir to offset this head drop. After some time, the downstream knife gate valve was closed. The final pressure head from the manometer was then recorded, and data acquisition process was stopped.

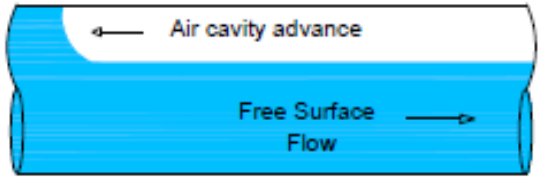

Figure 4.2 : Schematic of the air cavity advance after the downstream valve opening

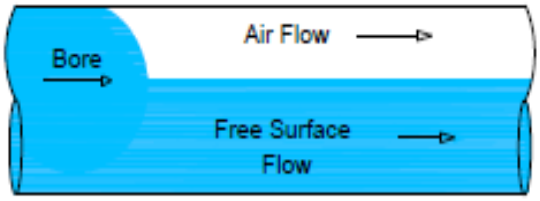

Figure 4.3: Schematic of the bore advance, in the experimental cases when the upstream valve opening did not result in air pocket formation

4.3. Data Analysis

Once the experimental runs and data collecting were complete, the process of data analysis was initiated. After videos were downloaded from the camera records, visual analysis was started to determine the advancing of air cavity and the bore through pipeline. The video recordings of each experimental were run frame by frame. The pipe is marked every 0.305-m. The time at which the air cavity or the bore reached each 0.305 m intervals was determined with the analysis of the frames. Given that the recording was performed in three separate camcorders, in order to observe air cavity and the bore movements throughout the experiment and to adjust the time differences between recordings, the Microsoft Windows Movie Maker program was used. By progressing frame by frame through the videos and determining the time at which cavity and bore reached the marks on the pipe at 0.305-m intervals it was possible to calculate the velocity of flow features by dividing the distance traveled over elapsed times.

During the data collection process, the pressure transducer setting was sampled at 200 Hz frequency. Piezo-resistive pressure transducers provides pressure values in voltage unit. During the data analysis process this voltage data was converted into pressure head readings by using a

calibration spreadsheet. The spreadsheet conversion assumed a linear relationship between voltage and pressure.

The results of the pressure transducers had noise in the signal that created difficulties in detecting the exact point of time at which the wave had moved over the sensor. To decrease this issue, a simple 5-point filter was used to smooth turbulence effects and help identify more clearly the moment when the pressure pulse occurred at each transducer by applying equation (4.1). The same 5-point filter was also used with ADV velocity measurements to reduce noise from the recorded velocity data.

$$P(n) = \frac{1}{5}\sum_{j=-2}^{j=2}(n + j) \tag{4.1}$$

Where P (n) is the filtered pressure at time n along the signal, and v (n + j) is the voltage that was recorded by the transducers at time n + j.

During the data collection process, the ADV, instrument for measuring velocity, was sampled at 25 Hz frequency. It was necessary some time adjustments in the ADV time column to match with the other experimental measurements during the tests.

4.4. Numerical Study

4.4.1 Air Pocket Entrapment Criteria

The appearance of air pocket entrapment depended on conditions on each experimental run, and it was typically associated with the cases with smaller D_C* and higher H_R* (defined as H_R/D). This is consistent with the observations by Li and McCorquodale (1999) and Kordyban (1990), who proposed theoretical criteria for appearance of air pocket entrapment during rapid filling of

closed conduits. Based on the experimental data, the values in their expressions were calculated and their criteria were also evaluated.

According to Li and McCorquodale (1999), the onset of SFI during rapid filling of closed conduits depended of an interface Froude-like parameter (F_I) that depended on the relative velocity between air and water and on the hydraulic water depth (area/free surface width) of the flow region in free-surface flow mode. If this value exceeded a critical value, defined as F_C, then SFI would occur during the rapid filling of the conduit. The formulas for both F_I and F_C are presented as follow in equations (4.2) and (4.3) respectively:

$$F_I = \frac{V_a + V_{FS}}{\sqrt{g h_{water}}} \geq F_c \tag{4.2}$$

$$F_c = K_f \sqrt{\frac{\lambda}{2\pi h_{water}}} \sqrt{\left(1 - \frac{\rho_{air}}{\rho_{water}}\right)\left(\frac{\rho_{water}}{\rho_{air}} \tanh\left(\frac{2\pi h_{air}}{\lambda}\right) + \tanh\left(\frac{2\pi h_{water}}{\lambda}\right)\right)} \tag{4.3}$$

Where V_a is the air velocity that is assumed to be numerically equal to the bore velocity, V_{FS} is the water velocity in free surface regime, h_{water} is hydraulic depth of water (*A/B*, with *B* as free surface width), h_{air} is hydraulic depth of air = $(D - h_{water})$ with K_f is a correction factor, ρ_{water} is the density of water, ρ_{air} is the density of air, λ is the wave length of the water wave. Given the specific conditions of this experiment, the displaced air velocity (assumed equal to V_a) underneath the cavity and the water velocity have the same initial direction, with both discharging downstream. The water velocity in the free surface decreases with the air pocket thickness, but for

the full discharge conditions it can be estimated as the same velocity of the air cavity with the equation (4.4) below:

$$V_{FS} = 0.54\sqrt{gD} \tag{4.4}$$

According to Kordyban (1990), the appearance of air pockets also depended on the maximum air velocity at the inside of the conduits that was used in the assessment of air-water instability in this study. Based on this study, Kordyban (1990) assumed that SFI would occur if the equation (4.5) expression is satisfied:

$$\rho_{air} V_a^2 \geq g(\rho_{water} - \rho_{air}) h_{air} \tag{4.5}$$

However, this relationship over-predicts the critical gas velocity by a factor of two. Therefore, the criteria for pocket appearance was modified as equation (4.6):

$$|V_a - V_{FS}| \geq \frac{1}{2}\sqrt{\frac{(\rho_{water} - \rho_{air}) g h_{air}}{\rho_{air}}} \tag{4.6}$$

4.4.2 Air Intrusion Velocity and Rigid Column Model

In this study, air cavity can be defined as an air intrusion into a closed pipe filled out with water when the closed pipe open to free surface. Benjamin (1968) work was primarily for air cavity intrusions into rectangular pipes, though the author included some discussion for circular cross-sections. In a related study, Townson (1991) presented a plot of the air cavity celerity for circular

pipes but did not provide equations for this advance. Vasconcelos and Wright (2008) derived the air cavity celerity C_{air} expression solution with equation (4.7):

$$\frac{C_{air}^2}{gD} = \left[\frac{\pi - \alpha - \sin\alpha\cos\alpha\,\pi}{\pi}\right]^2 \left[\frac{1 - \frac{1}{3\pi}(3\sin\alpha + 3(\pi - \alpha)\cos\alpha - \sin\alpha^3)}{\frac{\pi - \alpha + \sin\alpha\cos\alpha}{\pi}\left[2 - \frac{\pi - \alpha + \sin\alpha\cos\alpha}{\pi}\right]}\right] \quad (4.7)$$

Where the half angle is $\alpha = \cos - 1(2y/D-1)$ in which 2α is the angle subtended from the center of the pipe to the free surface.

The simulation of the advance of the pressurization interface can be attained for the case where air pockets do not appear through the application of a rigid column modeling approach. The expression enables for a comparison between calculated flow velocity after opening the upstream valve and measured flow velocity with the use of the ADV sensor. The initial rigid column model length was the region the upstream reservoir and the pressurization interface, formerly the leading edge of the cavity. Prior to the upstream valve opening, the water flow velocity within the column was negligible. The sudden opening of the valve introduced an upstream pressure head equal to height of reservoir that accelerated the column while increasing its length. The model represents a short period corresponding to the advance of a pipe filling bore until it reached the downstream end of the pipe. The model is not representative of the cases in which an air pocket would form, unlike the model that was presented by Li and McCorquodale (1999).

Wylie et al. (1993) presented the mathematical formulation of the rigid column approach. One of the key simplifications that is introduced is that it neglects spatial variations of the pressure gradient term in the momentum equation. The resulting expression is thus simplified from the original system of partial differential equations into a much simpler ordinary differential equation that solve the evolution of the flow rate within the advancing rigid column. The use of the rigid

column modeling approach presented in equations (4.8) and (4.9) offered an independent means of calculating the flow velocities during the early stages of the flow. Another ordinary differential equation that results from the approach is the update of the rigid column length L_c that depends directly on the calculated *Q*, as well on the difference between the pipe cross-sectional area $A_{pipe} = \frac{\pi}{4} D^2$ and the area of the free surface flow A_{fs}:

$$\frac{dQ}{dt} = \frac{gA_{pipe}}{L_c}\left[H_R - \frac{D}{2} - Y_{dw} - \left(K + f\frac{L_c}{D} - 1\right) \cdot \left(\frac{Q^2}{2gA_{pipe}^2}\right)\right] \tag{4.8}$$

$$\frac{dL_c}{dt} = V_a = \frac{Q}{A_{pipe} - A_{fs}} \tag{4.9}$$

Where Y_{dw} is the depth of the centroid of the cross section at the downstream end of the rigid column (i.e. bore); *K* is the combined local loss due to the pipe entrance and opened knife gate valve, assumed as 1.5; *f* is the friction loss coefficient, assumed as 0.025. Since it is not possible to calculate air cavity thickness, the values used for air cavity thickness were obtained from the CFD model results obtained in a earlier investigation presented by Yasemin Eldayih, and presented in table 5.3. Using these CFD-derived thickness values, it was possible to compute Ydw and Afs that are used in equations 4.8 and 4.9. An schematic illustrating the key variables of the rigid column model is presented in Figure 4.4.

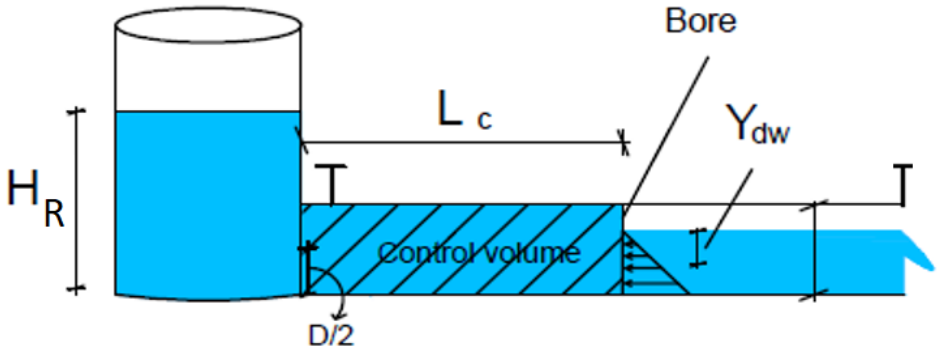

Figure 4.4: Schematic illustrating of the rigid column model

Chapter 5. Results and Discussion

This chapter presents results and discussions about this experimental study in rapid filling of closed conduits and the possibility of air pocket formation due to SFI. For the presentation of the results, the reservoir head and discharge opening where normalized by the pipe diameter *D*. Likewise, the pressure head values *H* are normalized by *D*, whereas velocity and celerity values are normalized by$\sqrt{gD}$. Finally, time measurements, which are initiated when the downstream valve opened, are normalized by $L/\sqrt{gD}$. The reservoir head was normalized by pipe diameter *D*, and referred to H_R*, and so was the gap in created by the obstruction weir, referred to as *Dc**. Starred will refer to normalized variables. In the experimental study, air-pocket entrapment was investigated in 12 different cases involving the rapid filling of the pipe, with and without restriction weirs and with three levels at the upstream reservoir. Experiments was repeated two times, so the results for both repetitions were presented in this chapter.

5.1 SFI threshold criteria results

After the downstream valve opening, an air cavity propagates in the horizontal pipe which is shown in Figure 4.2 with the snapshots and in Figure 5.1 with the sketch. In Figure 5.1, video recording snapshots presented that illustrate the air cavity leading edge advance 8 seconds after the downstream valve was opened. It can be easily seen in the figure that the changes in thickness,

shape, and the location of the air cavity depended on height of weir and resulting values of *Dc**, with air cavity celerity decreasing with smaller *Dc**. This is consistent with the expression presented by (Vasconcelos and Wright 2008) relating air pocket thickness and related celerity.

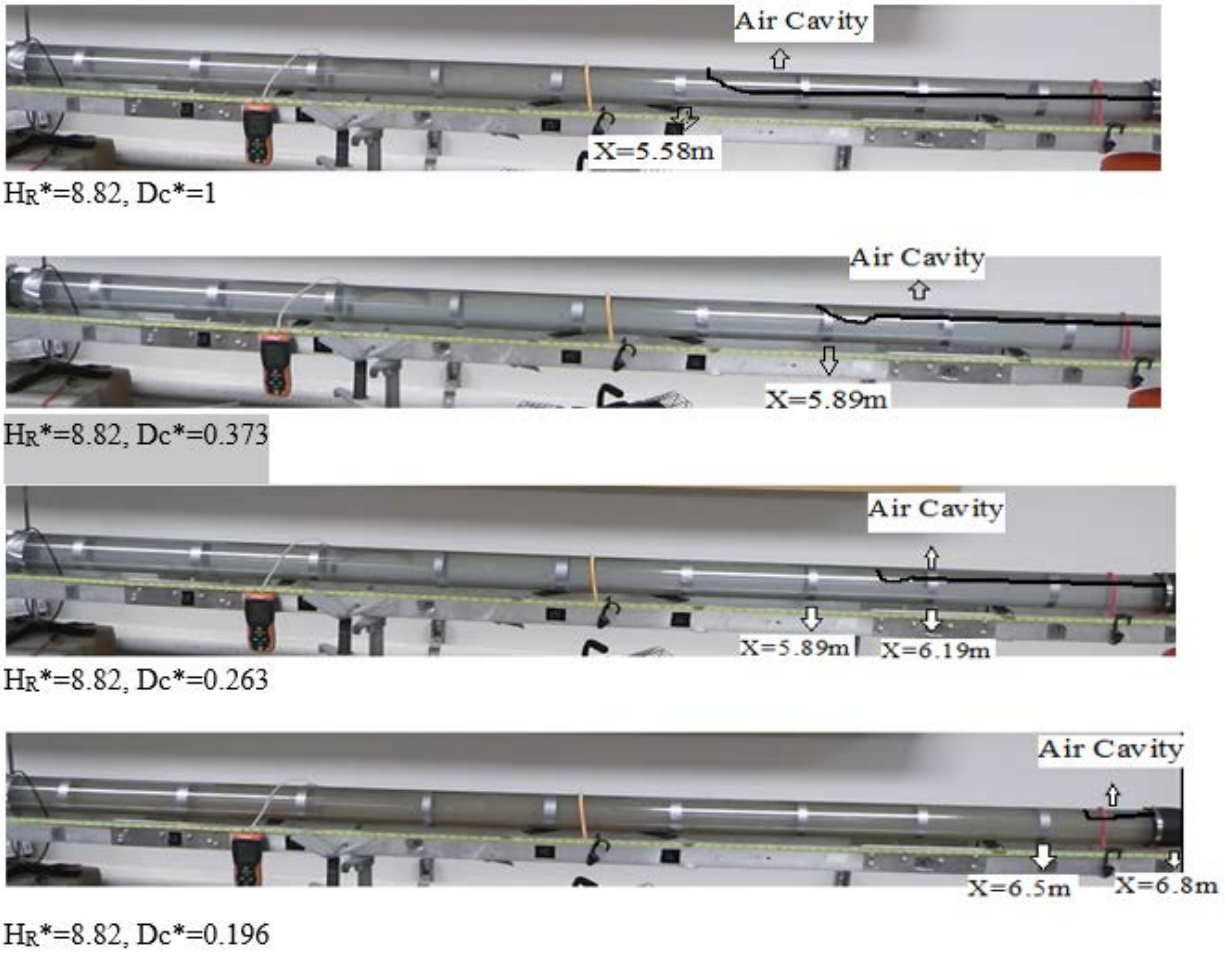

Figure 5.1: Air cavity leading edge advance 8 seconds after the downstream valve opening.

Once the cavity approached the upstream end, the upstream knife-gate valve was opened, creating pressurized conditions. As pointed out earlier, there are two possible outcomes that occurred following this valve opening: either air pocket entrapment occurred due to SFI or the propagation of otherwise a pipe-filling bore. These outcomes are outlined in Table 5.1, along with the predictions by the theoretical threshold criteria proposed by (Li and McCorquodale 1999) and

by (Kordyban 1990). In the table s, 'EXP' refers experimental observes that obtained by watching the records from camcorder records. 'LM' and 'KO' refers the theoretical result about in which condition pocket entrapment is seen when SFI occur according to (Li and McCorquodale 1999) and (Kordyban 1990).

Table 5.1. Outcome of the rapid filling of the conduit based on Li and McCorquodale (1999) threshold (LM), Kordyban (1990) threshold (KO) and experimental observations.

Dc*	Results for	H_R*		
		2.94	5.88	8.82
1.000	EXP	Bore	Bore	Bore
	LM	Bore	Bore	Bore
	KO	Bore	Bore	Bore
0.373	EXP	Bore	Bore	Bore
	LM	Bore	Air Pocket	Air Pocket
	KO	Air pocket	Air Pocket	Air Pocket
0.265	EXP	Bore	Air Pocket	Air Pocket
	LM	Bore	Air Pocket	Air Pocket
	KO	Bore	Air Pocket	Air Pocket
0.196	EXP	Air Pocket	Air Pocket	Air Pocket
	LM	Air Pocket	Air Pocket	Air Pocket
	KO	Bore	Air Pocket	Air Pocket

Experimental measurements match with LM under all other conditions except (Height of weir = 0.038m and Height of reservoir=0.6m and 0.9) conditions. Also, the greatest discrepancy with experimental measurements was noticed with the modified Kordyban threshold criterion.

5.2 Pressure head results

Figure 5.2, 5.3 and 5.4 presents measured pressures resulting from each tested condition obtained with the piezo-resistive pressure transducer located at x=3.18 m. During the earlier stages of the experimental run, after the downstream air valve was opened, values of the normalized pressure head at the transducer are near unity, that is pressure head is near the pipe diameter. As it can be seen in Figure 9 for the fully opened weir height case only, there is a water level drop created by the air cavity as it passed through the transducer location. This was not noticed for other cases because the cavity thickness was smaller than the transducer sensitivity to detect pressure changes created by the cavity motion.

A sudden pressure rise is noticed afterwards due to the arrival of the pressurization front caused by the opening of the upstream valve. In some cases, this front was characterized by a pipe-filling bore, but even when air pockets appeared in the solution the pressure rise did occur. In some cases, shortly after the passage of the presserurization inferface through the transducer location, high-frequency pressure oscillations characterized by pressure drops were noticed. For all cases (except D_C^*=0.265 and H_R^*=2.94) these cases corresponded to conditions where air pockets were entrapped. These spikes are attributed to air pockets being rapidly released at the downstream end of the apparatus, dropping the pressure in the system in this process.

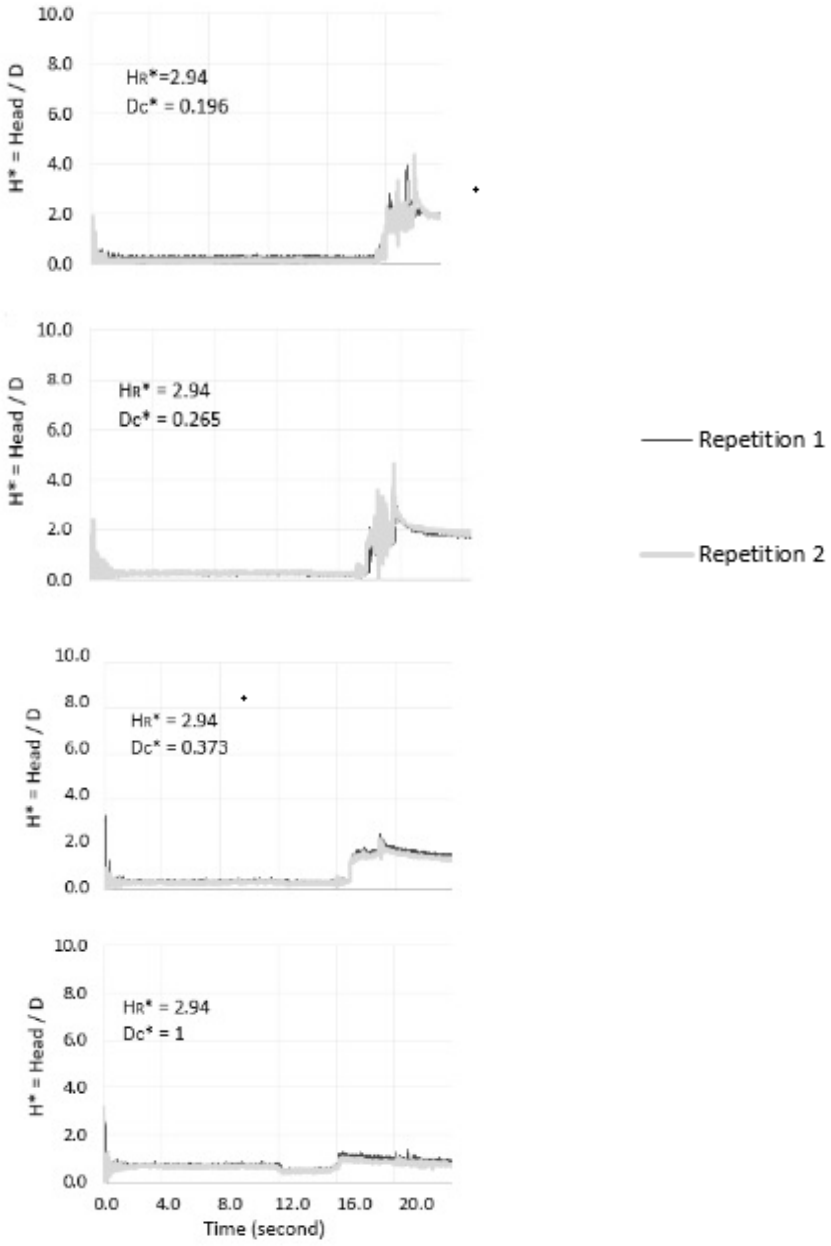

Figure 5.2: Experimental pressure head results in the case of 0.305 m reservoir head and three different weir height (D_C values of 0.02 m, 0.027 m, 0.038 m and 0.102 m).

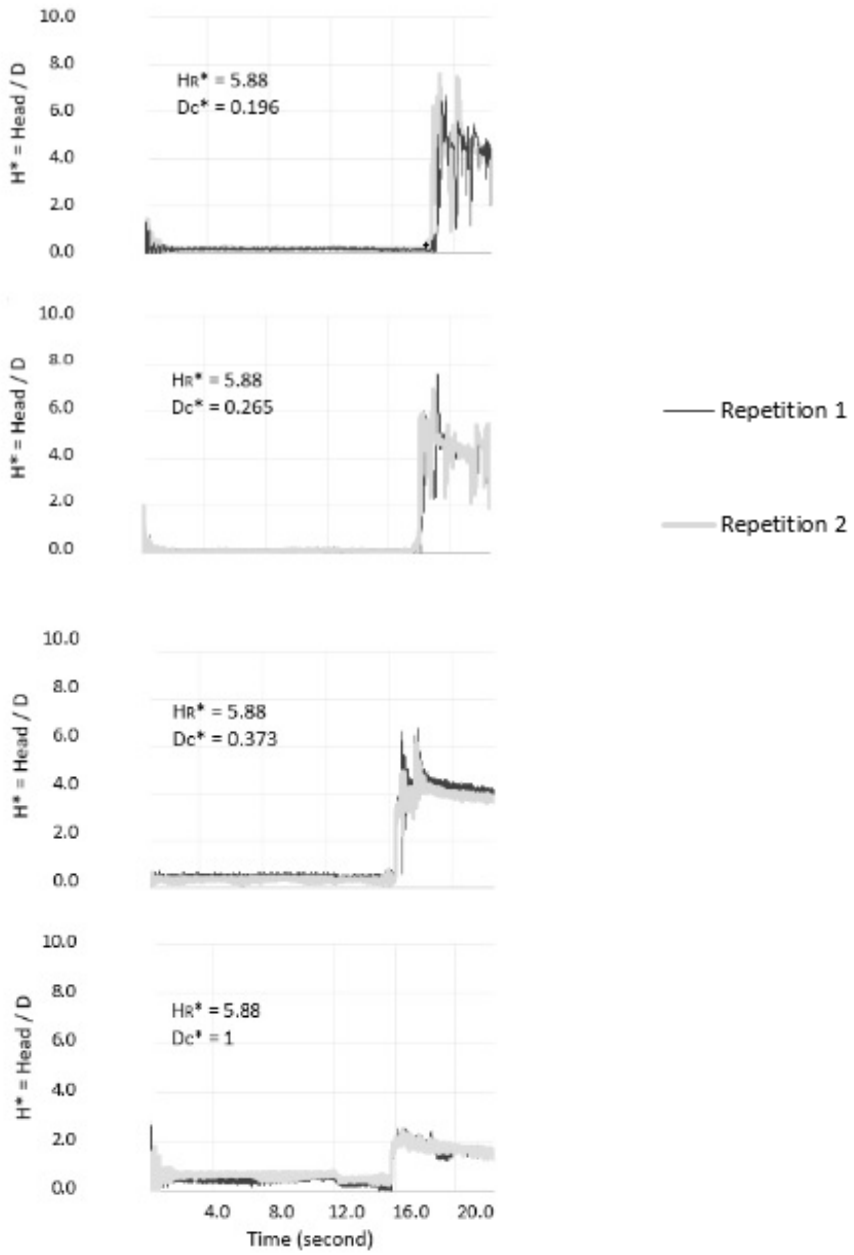

Figure 5.3: Experimental Pressure Head Results in the case of 0.61 m reservoir head and three different weir height (D_C values of 0.02 m, 0.027 m, 0.038 m and 0.102 m).

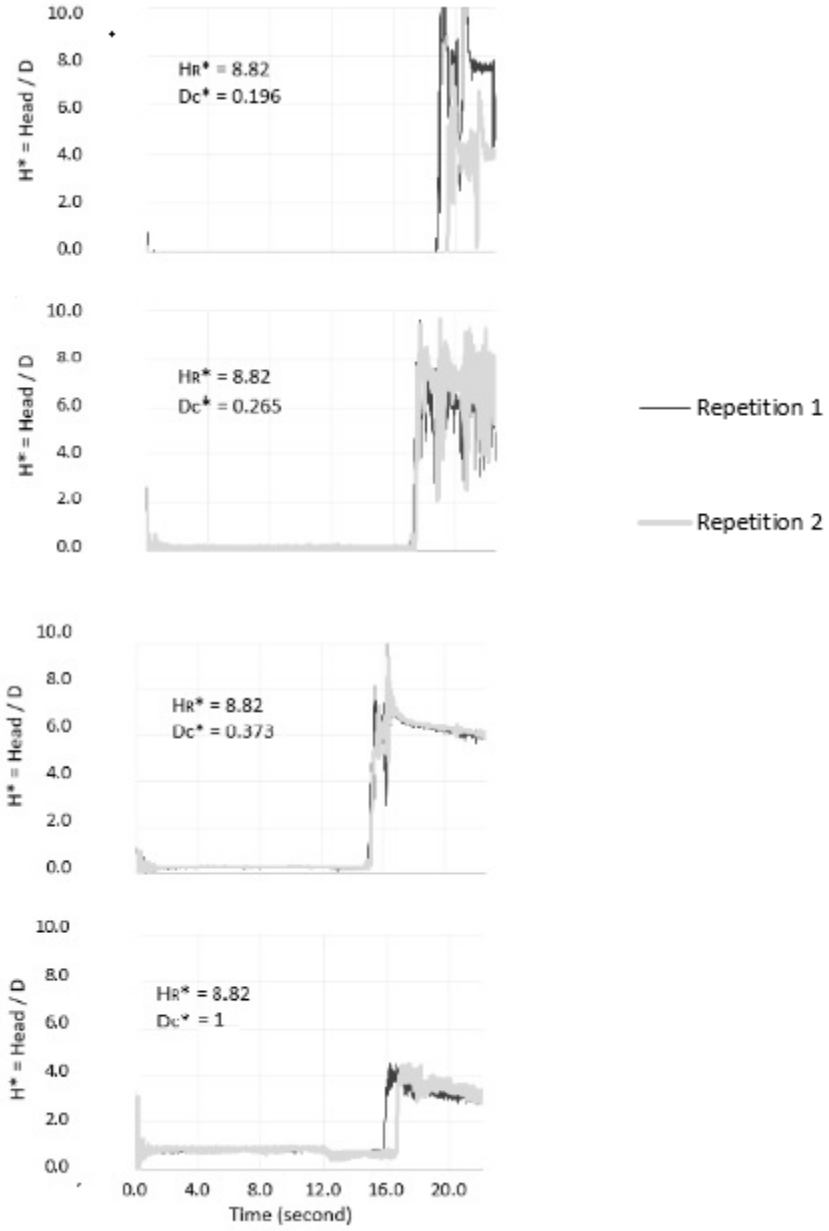

Figure 5.4: Experimental pressure head results in the case of 0.915 m reservoir head and three different weir height (D_C values of 0.02 m, 0.027 m, 0.038 m and 0.102 m).

5.3 Characteristics of air cavities and inflow fronts

Figures 5.5, 5.6 and 5.7 present measured velocity resulting from each tested condition from the ADV grouped by reservoir pressure head. In the earlier stages of the flow, following the downstream valve opening, there is no noticeable velocity in the water phase until the arrival of the air cavity. As the cavity arrives at the location where the ADV sensor is placed, there is an increase in the velocity that can be estimated through a local continuity equation expression

$$V_{water} = \frac{C_{air} A_{cavity}}{\frac{\pi}{4} D^2 - A_{cavity}} \qquad 5.1$$

Where $V_{water}$is the velocity measured with the ADV, and A_{cavity} is the cross sectional area of the cavity. With smaller D_c^* values, the cavity thickness and A_{cavity} values decreased along with C_{air}, as is indicated in equation 4.7. For the smallest air thickness, the velocity was so small that the ADV did not measured it, but then *Dc** was 1.0, the value for V_{water} equaled C_{air}, as it would be anticipated.

Shortly after the upstream valve opening, a jump occurs in velocity magnitude with the advance of the pressurization interface. This jump was more pronounced with increased values of height of reservoir and height of weir. Some small spikes in velocity immediately after this jump were caused by the turbulent nature of the flow, as there were no detedted signs of the expulsion of entrapped pockets through the downstream end with the velocity results. As is shown in Figure 5.5, 5.6 and 5.7, the final water velocity increased with larger D_C* values, as it would be expected since the degree of flow obstacle would have decreased. The estimated value for the pipe-filling bore celerity was calculated based on the elapsed time for the bore displacement until it reached

the downstream knife-gate valve and is presented in Table 5.2. There is some uncertainty in this estimate due to the limitations on the camera as to how sharp be the image of the bore front. These celerity values normalized by $\sqrt{gD}$ are reported with respect to the fixed experimental apparatus. As it seen, bore celerity values increased with upstream reservoir head.

Table 5.2: Normalized averaged pipe-filling bore celerity.

H_R*	D_C*			
	1.00	0.37	0.26	0.20
2.94	1.89±0.1	2.5±0.1	3.4±0.2	NA
5.88	2.3±0.1	3.5±0.2	NA	NA
8.82	2.4±0.1	NA	NA	NA

In Table 5.3, some air cavity characterizes were presented. Also, table 5.3 was included velocity under the cavity that refer a rate of Qair/Afs the bore velocity passed the cavity and push it to downstream end. Where Qair is the discharge of the cavity and Afs is the free surface area. For cases involving SFI, the pressurization front caused by the rapid filling process came downstream, leaving pockets behind (or within the pressurized flow region). Theoretical air cavity celerity values and measured air cavity values very consistently. Air cavity thickness and celerity values increases as downstream opening values increase. Air cavity advance values are the length of the column values for rigid column modeling that calculates the length of the pipe minus max air cavity advance.

Table 5.3: Air cavity characteristics

D_C*	Theoretical air cavity celerity/$(gD)^{0.5}$	CFD result for average air cavity thickness/D	Measured Air Cavity Celerity/$(gD)^{0.5}$	Air cavity advance/L prior to upstream valve opening	Velocity under the cavity /$(gD)^{0.5}$	Estimated Air Cavity Thickness /D
1.0	0.50	0.47	0.497± 0.006	0.76	0.497±0.005	0.53
0.373	0.47	0.19	0.480±0.003	0.71	0.478±0.002	0.22
0.265	0.44	0.14	0.431± 0.003	0.67	0.425±0.002	0.19
0.196	0.39	0.11	0.360± 0.006	0.63	0.350±0.006	0.12

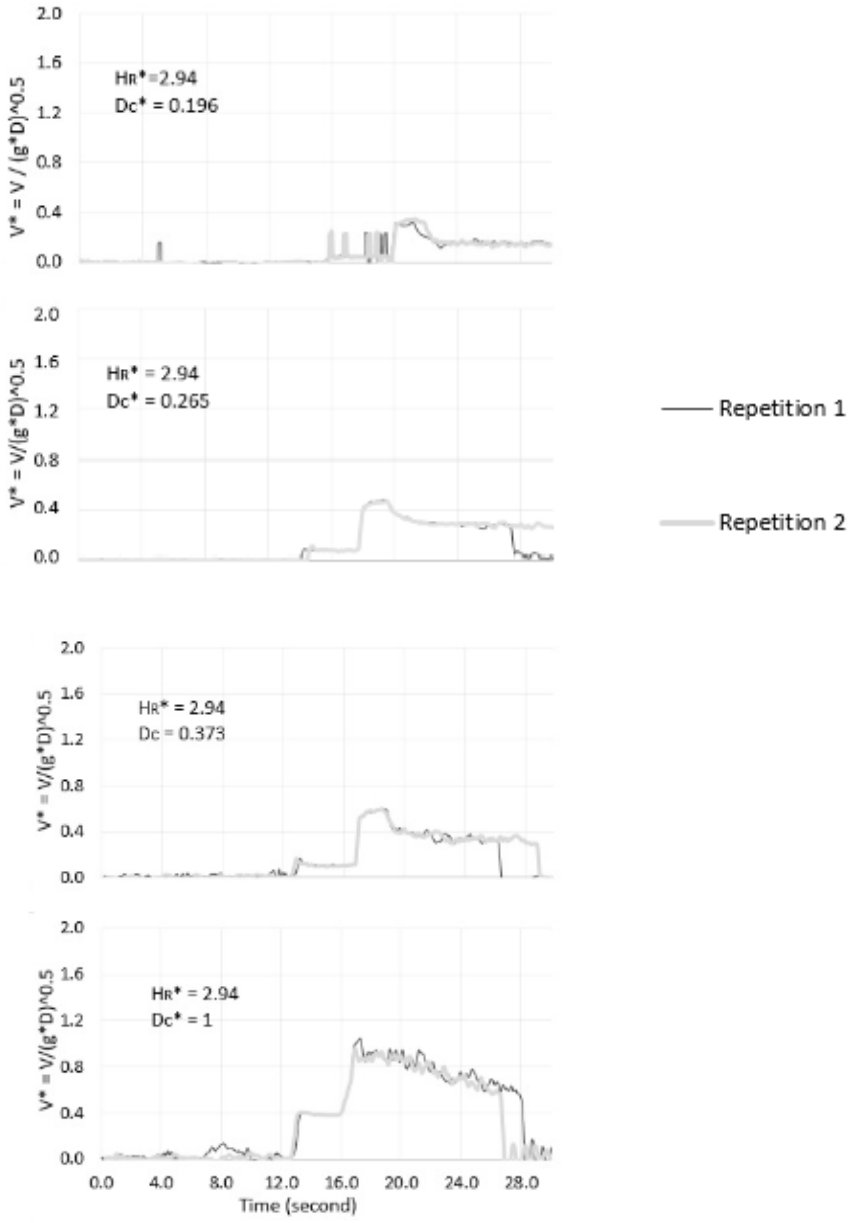

Figure 5.5: Experimental velocity results in the case of 0.305 m reservoir head and three different weir height (0.02 m, 0.027 m, 0.038-m and 0.102 m)

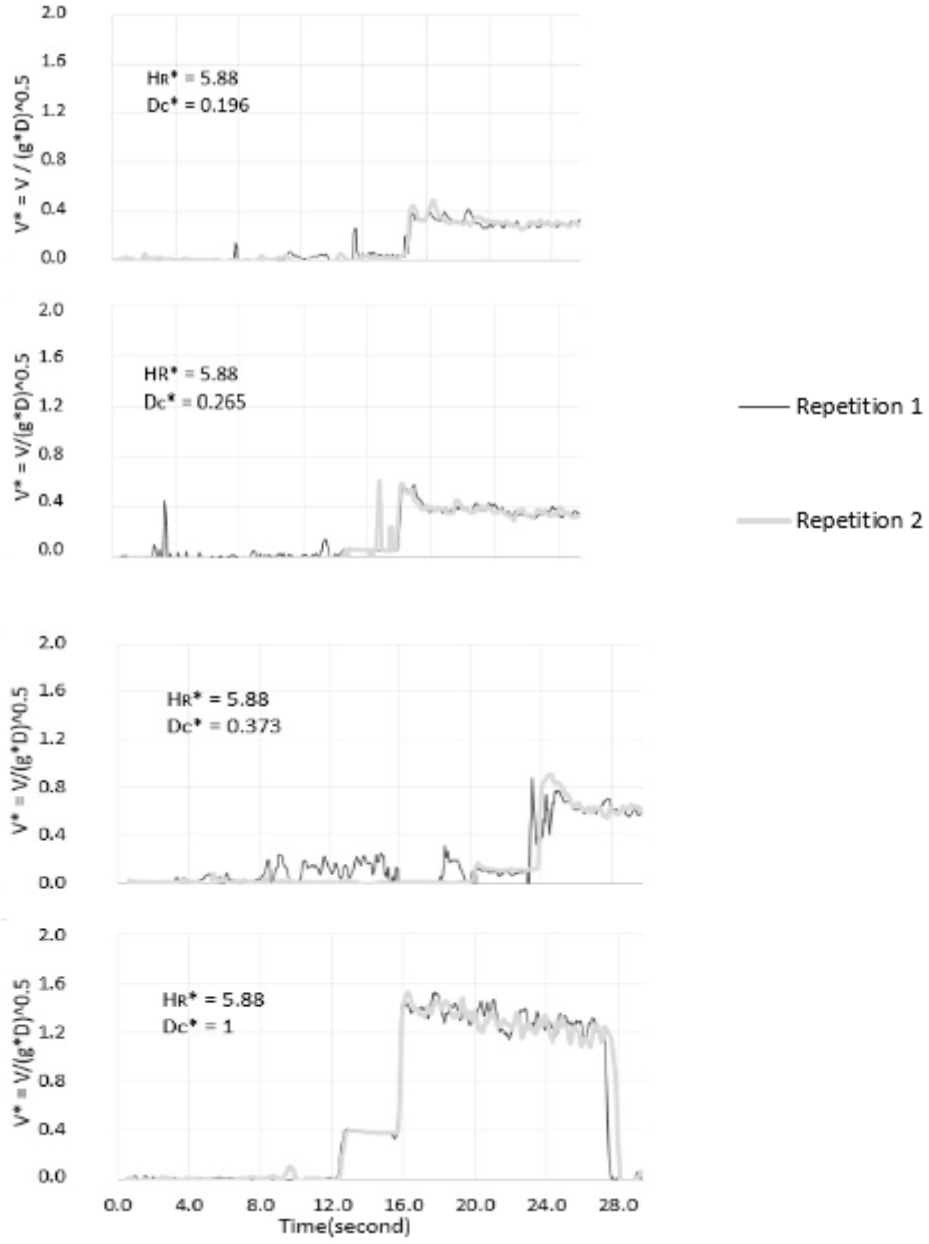

Figure 5.6: Experimental velocity results in the case of 0.61 m reservoir head and three different weir height (0.02 m, 0.027 m, 0.038 m and 0.102 m)

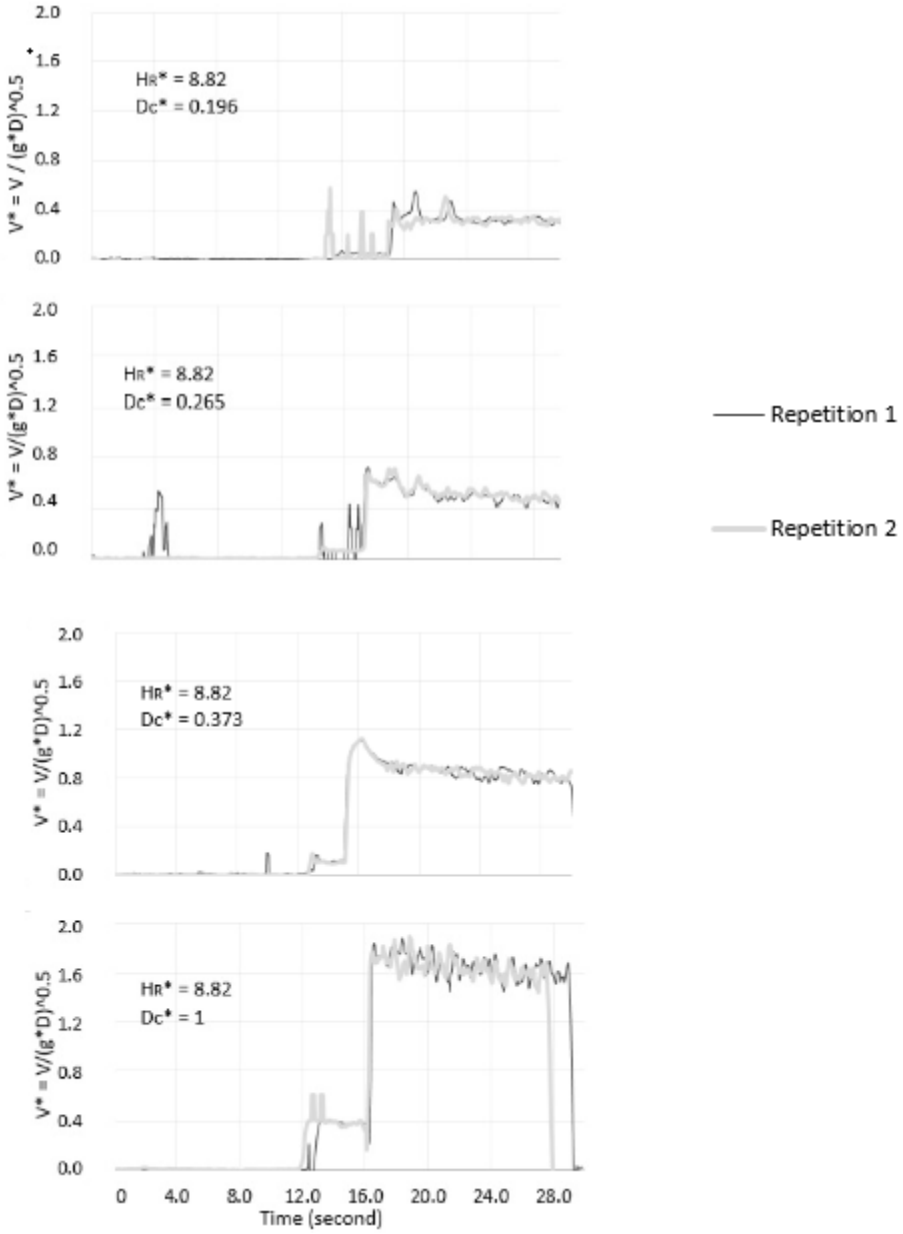

Figure 5.7: Experimental Velocity Results in the case of 0.915 m reservoir head and three different weir height (0.02 m, 0.027 m, 0.038 m and 0.102 m)

A comparison between measured velocity and the predictions yielded by the Rigid Column model using $V=Q/A_{pipe}$ for the flow velocity sampled near the location of the Vectrino ADV sensor is presented in Figure 5.8. The use of a rigid column formulation in this study intended to provide an alternative means to estimate the growth in water velocity following the opening of the upstream valve. The rigid column modeling approach is applied during the brief period between the opening of the upstream valve and the arrival of the inflow front at the downstream end of the pipe.

The method has important limitation such as the inability to account for the appearance of air pockets and their pressurization. Air pocket formation should lead to a decrease on water column acceleration during the rapid filling stage of the experiment. Thus, for the experimental cases where air pockets were not reported, the rigid column model results should be closer to the experimental data. Also, it must be noticed that equations 4.8 and 4.9 are unable to describe the advance of the air cavity prior following the initial downstream valve opening.

Despite of these limitations, the rigid column method was considered as a simple and quick estimate of the water column acceleration for the pressurization front following the opening of the upstream valve. The alternative for this method could be the approach proposed by Li and McCorquodale (1999), despite of various simplifying assumptions, or calculation through CFD modeling tools.

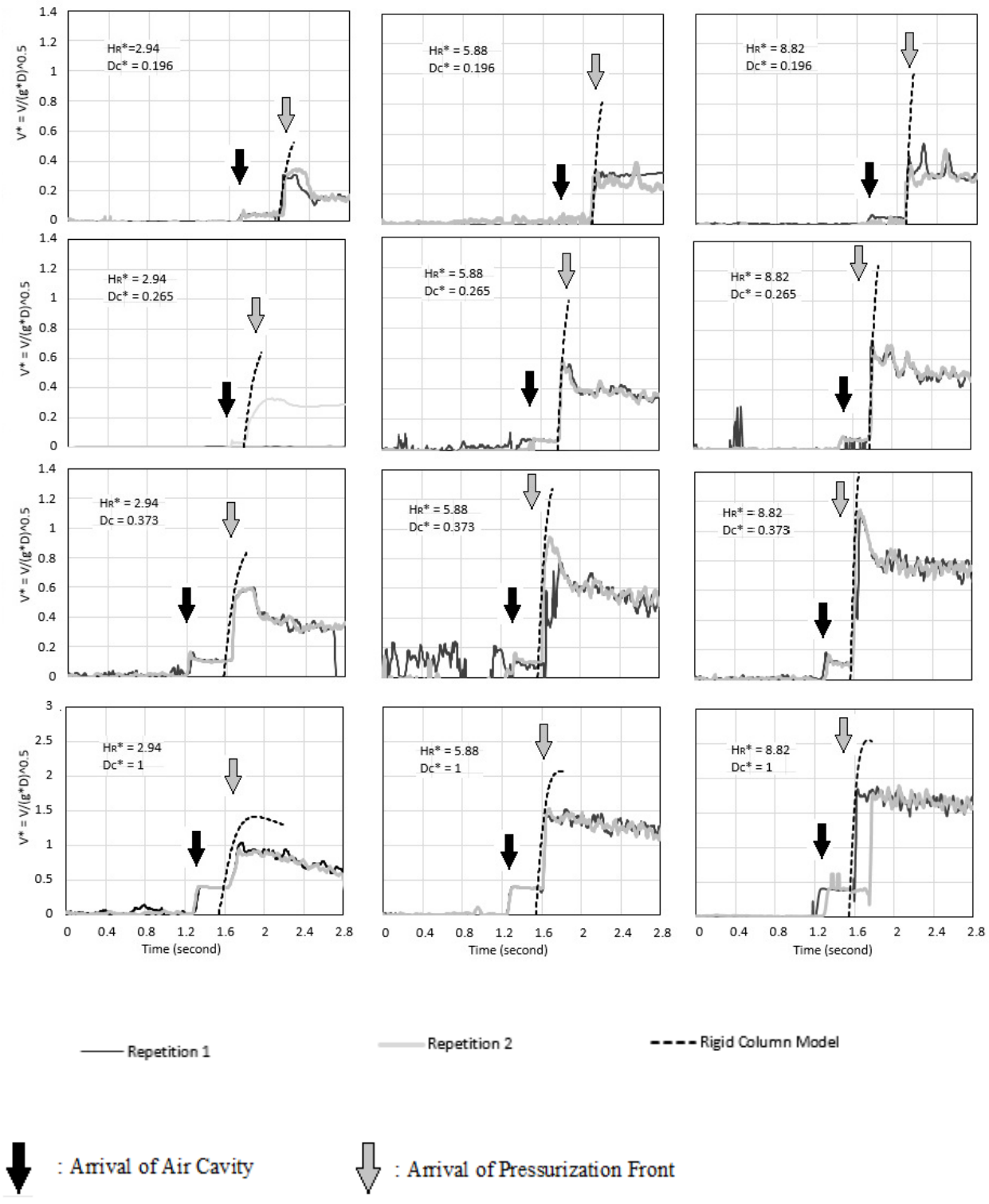

Figure 5.8: Comparison between normalized velocity (V*=V/(g D)0.5) measured in experiments and rigid column model velocity values for all tested conditions.

5.4 Description of filling process

The purpose of this section is to compare the advance of a pressurization bore front and the pressurization interface when SFI occurs. Figure 5.9, 5.10 and 5.11 presents video recording snapshots that illustrate the different instances of air pocket entrapment and rapid filling bore for the case $Dc^*=0.26$ $H_R^*=8.82$, $Dc^*=0.196$ $H_R^*=8.82$ and $Dc^*=0.196$, $H_R^*=5.88$, respectively. The snapshots were taken using the camera nearest to the downstream end.

In Figure 5.9, an interesting outcome is noticed in that the air pocket formation “shifted” the pressurization interface position ahead of the pipe-filling bore. This new pressurization interface continued to advance rapidly and causing another air pocket entrapment ahead of it. Li and McCorquodale (1999) also suggested this outcome. Such results indicate that multiple air pocket entrapment formation is theoretically possible with the SFI mechanism, which is very relevant in the context of rapid filling pipe and air-water interaction research. Sometimes in experiments the formed pockets merged to the other pockets' tail, but this could be a result of the limited longitudinal length of the experimental apparatus. Experimental observations indicate that most volumes of air pockets are discharged at the downstream end, but a residual amount of air tended to merge and become a long thin pocket.

Figure 5.10 presents snapshots from $Dc^*=0.196$ $H_R^*=8.82$ condition. According to this case, pressurization interface position follows the pipe-filling bore and multiple air pocket entrapment in the same time was not observed from the records. Based on observations from the records air pockets’ thickness are smaller than half of the diameter and mostly merged and became a long thin pocket without discharging from the downstream.

Figure 5.11 show no air pocket entrapment case, and the pressurization front advancing in fully open height of weir and 0.61-m upstream reservoir head case.

Figure 5.12, 5.13 and 5.14 presents movement of air cavity and pressurization front and shows the air cavity and pressurization front advance each 0.305 m. The locations of air cavity and pressurization front were tracked after the downstream valve opening and initiated the water outflow. The measured air cavity celerity and the pressurization front advance velocity were influenced both by the air pocket thickness and by the pressure head in the reservoir.

Table 5.4 present normalized pressurization interface celerity. These values were obtained by watching camera records based on displacement and elapsed time. These results are consistent with theory, in the sense that the pressurization interface advanced more rapidly in cases when the air pocket thickness was smaller (lower D_C^*). Also, as it could be anticipated, higher pressure levels at the reservoir yielded faster pressurization interface celerity.

Table 5.4: Pressurization interface celerity normalized by $(gD)^{0.5}$

H_R*	D_C*			
	1.00	0.373	0.263	0.196
2.94	1.67±0.01	2.60±0.05	3.5±0.05	4.0±0.05
5.88	2.49±0.01	3.80±0.02	4.6±0.05	5.03±0.06
8.82	2.81±0.01	4.06±0.05	5.04±0.06	5.40±0.06

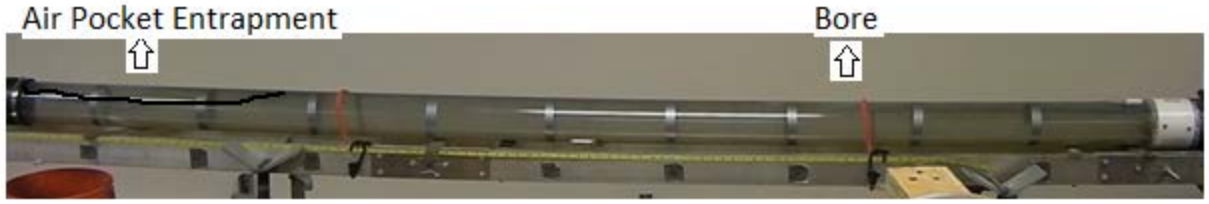

T=16.94 second

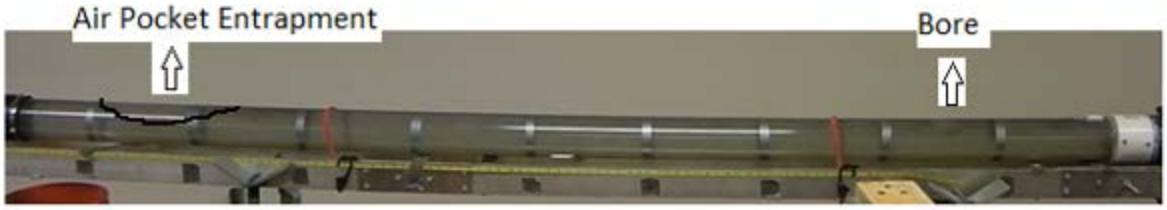

T=17.00 second

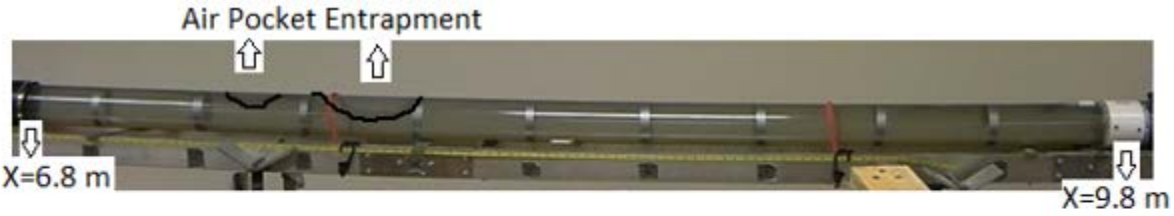

T=17.04 second

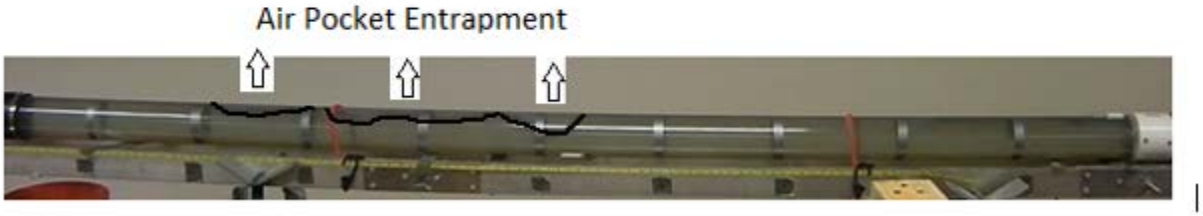

T=17.06 second

Figure 5.9: Outcome for 0.027 m opening of downstream and 0.915 m upstream reservoir head

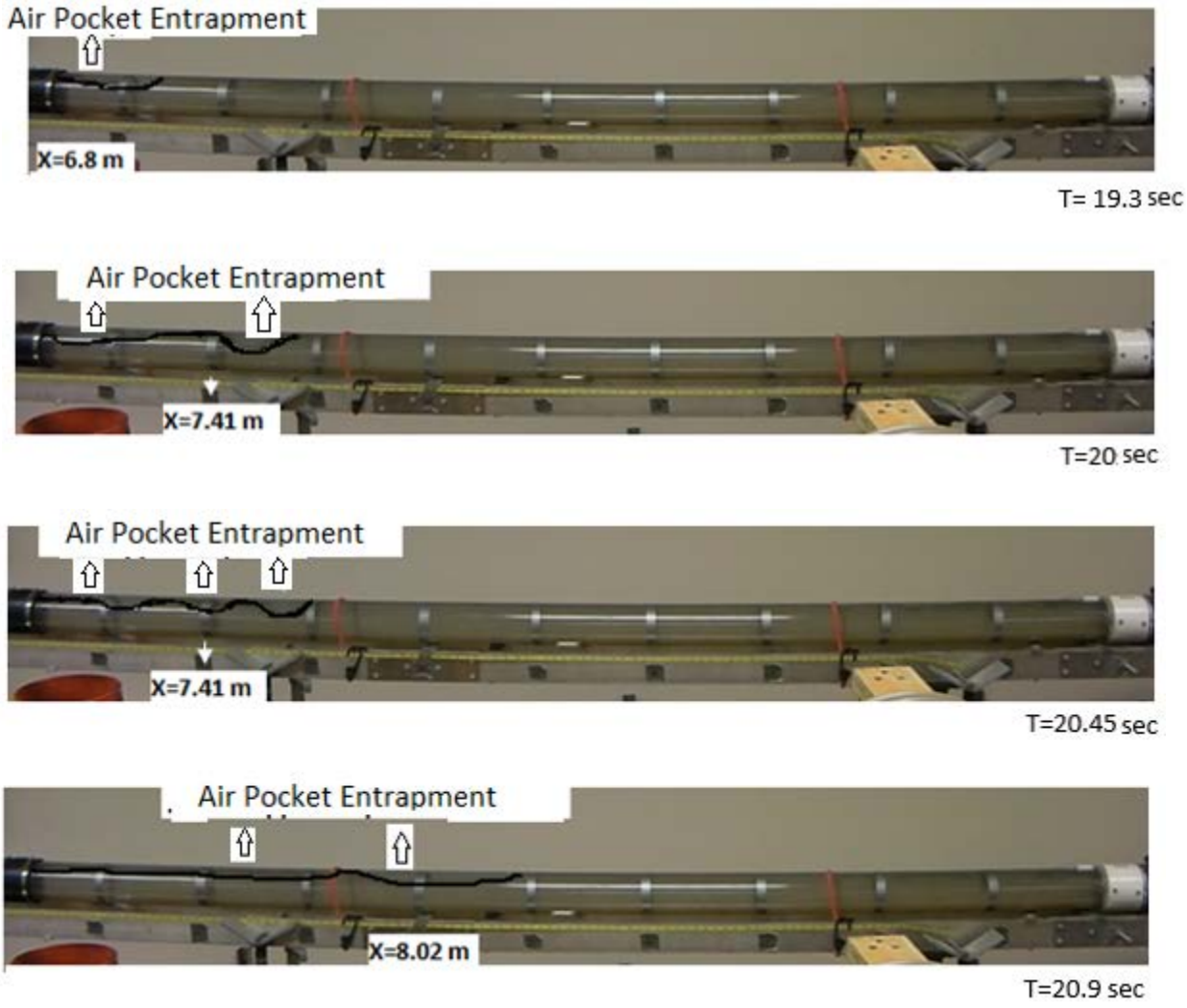

Figure 5.10: Outcome for 0.02 m opening of downstream and 0.915 m upstream reservoir head

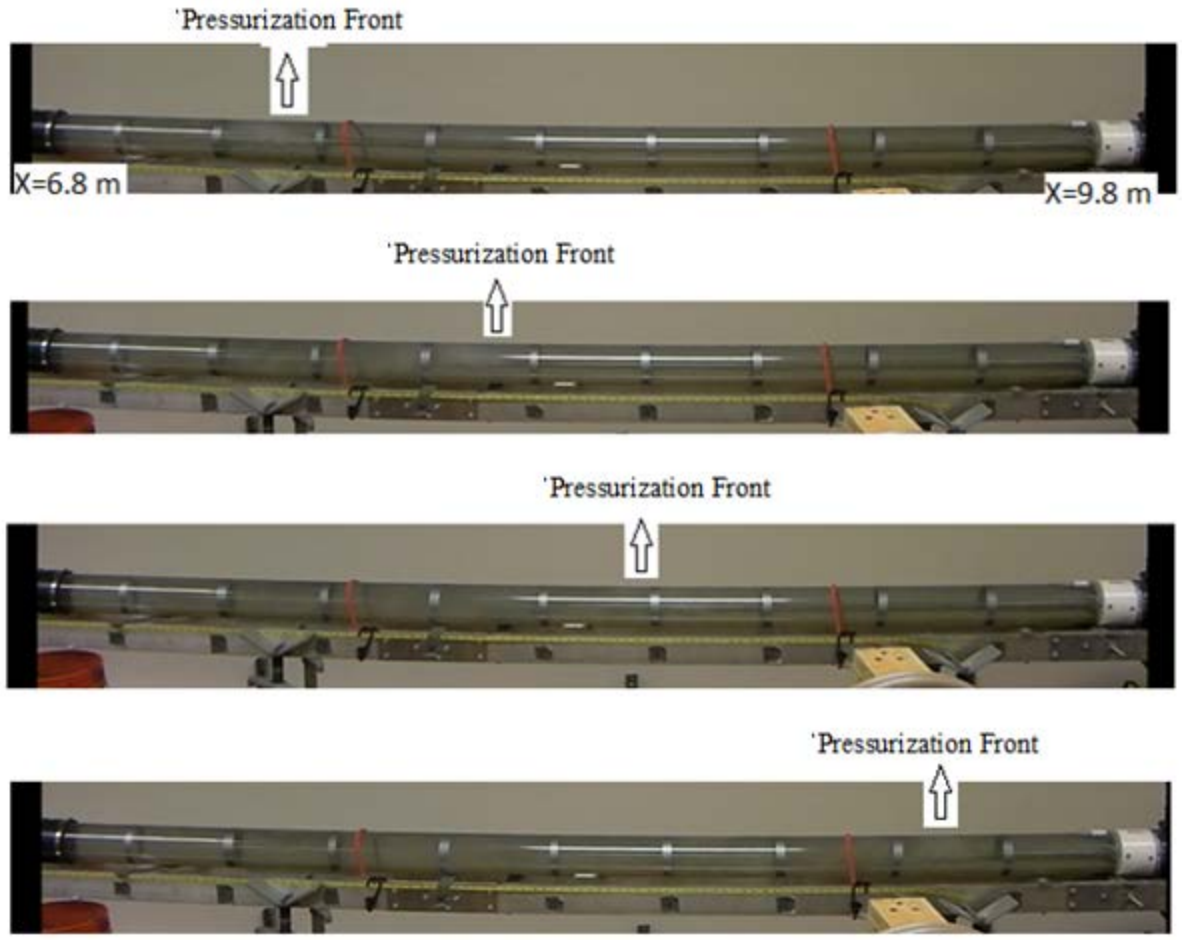

Figure 5.11: Outcome for fully opening of downstream and 0.61 m upstream reservoir head

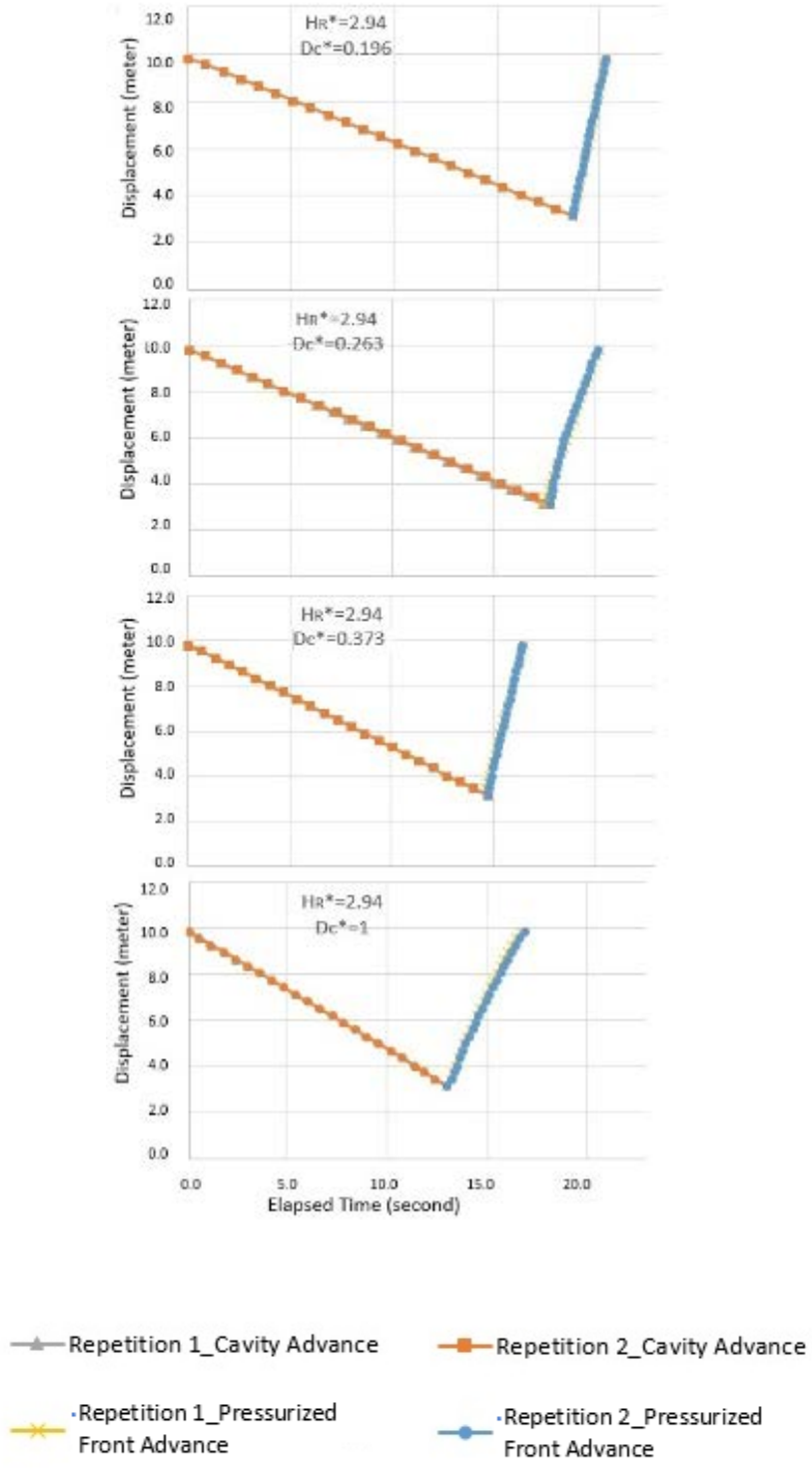

Figure 5.12: Movement of air pocket and pressurized front for H_R^*=2.94

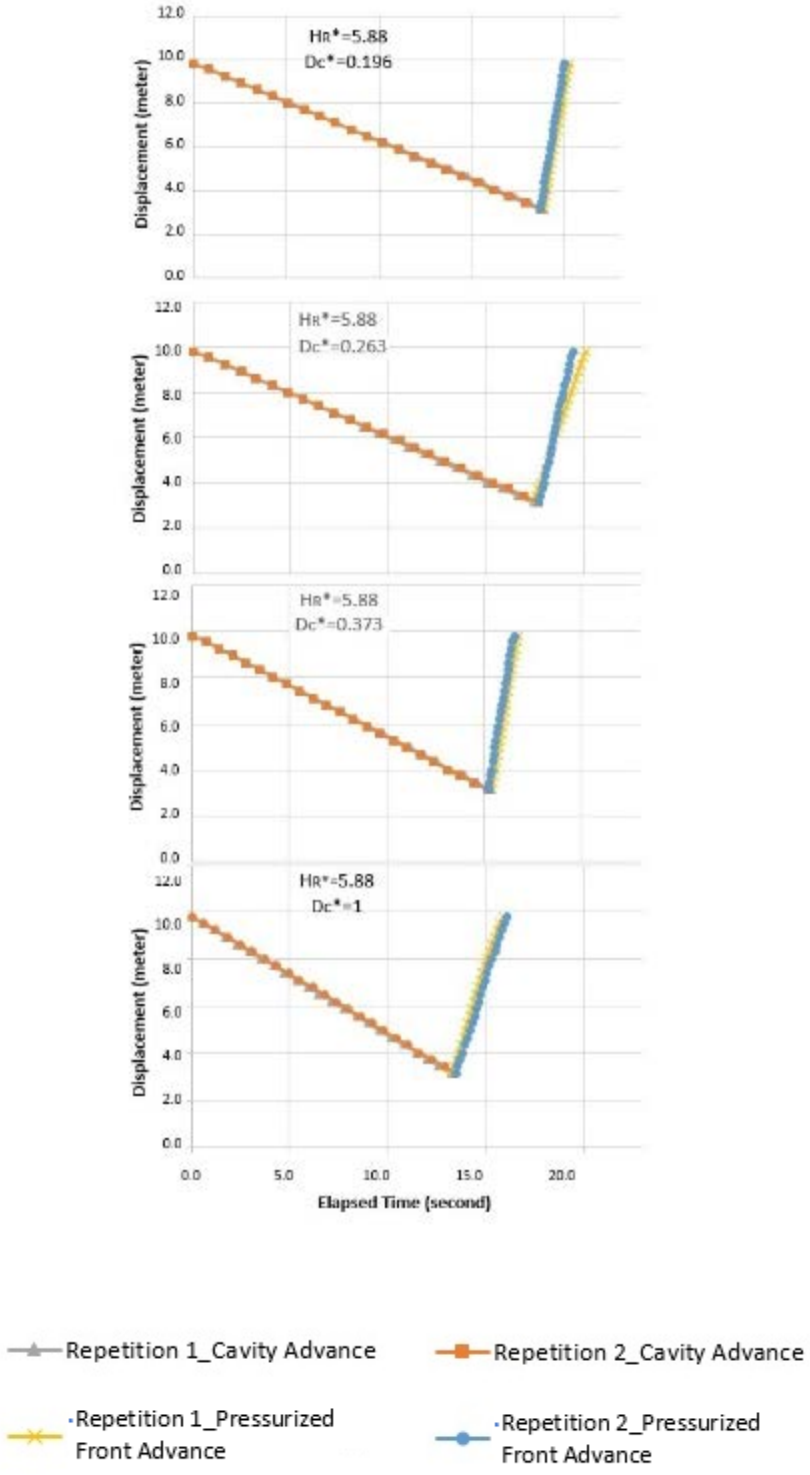

Figure 5.13: Movement of air pocket and pressurized front for H_R^*=5.88

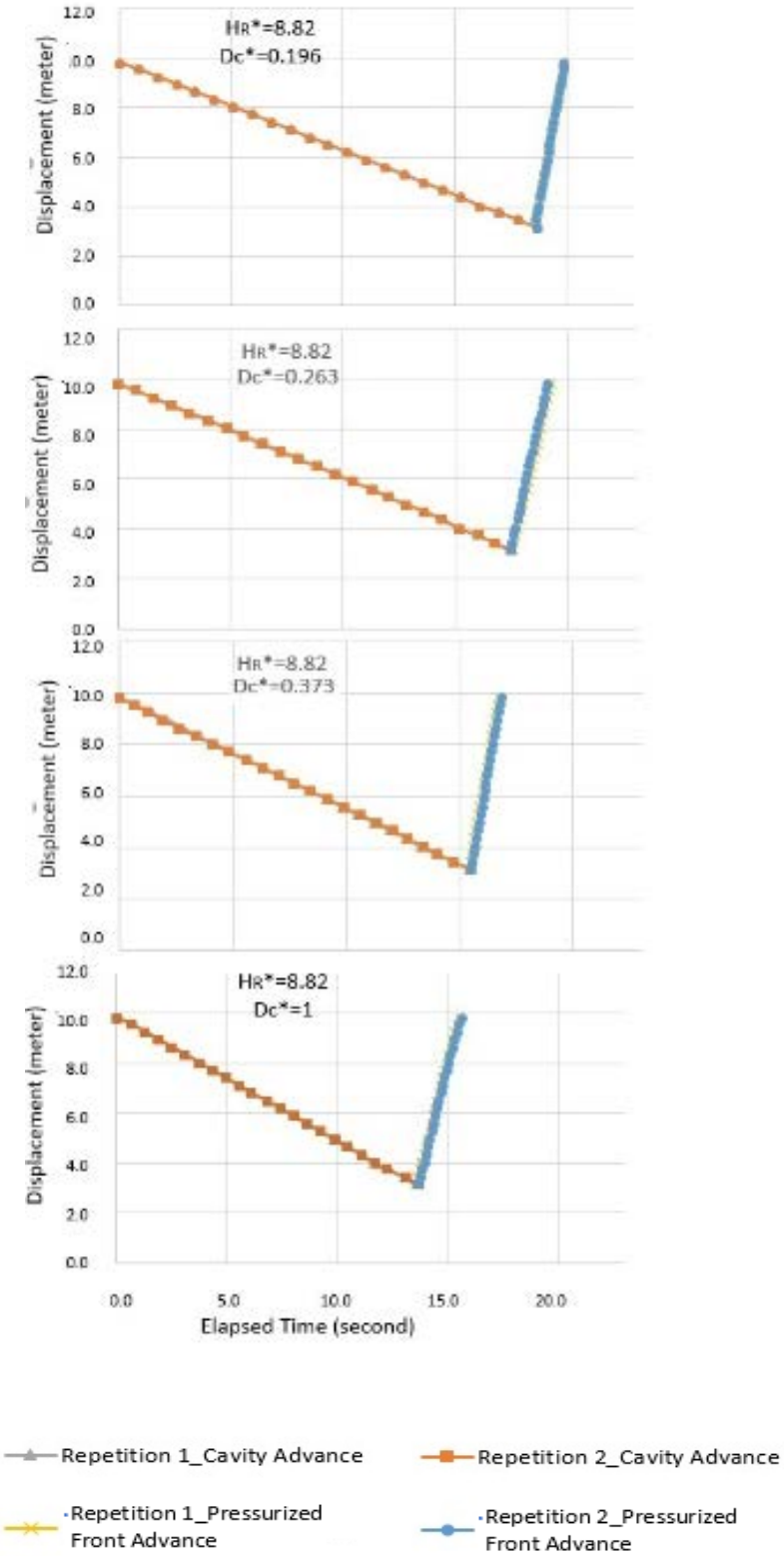

Figure 5.14: Movement of air pocket and pressurized front for H_R^*=8.82

Chapter 6. Conclusions

Air pocket entrapment is an important issue in stormwater sewers and tunnels undergoing rapid filling. While it is currently acknowledged that entrapped air pockets can result in surging, geysering and other operational issues, mechanisms for air pocket entrapment are still poorly understood. The focus of the present work was to investigate characteristics of air pocket entrapment created by shear flow instabilities (SFI) caused by the relative motion of air and water phases during rapid filling conditions. An innovative apparatus was used that enabled the development of air cavities with varying thickness and a rapid filling with different flow rates. As result, various air pocket entrapment conditions were reproduced in laboratory conditions, making this the first systematic experimental investigation on SFI.

This study involved the development of an innovative experimental system that enables a systematic variation of rapid filling conditions (changed diameter rates and pressure head), both in terms of characterizes of initial air phase layer and the pressurization interface advance. The experimental procedure was included the three upstream reservoir levels and four different weir opening values yielded a total of 12 unique experimental conditions. Each of these conditions were repeated at least 3 times to ensure consistency of experimental measurements.

According to the experimental results, the likelihood of air pocket formation increased with smaller air pocket thickness and faster pressurization interface advancement values. For at 0.02 m

downstream opening condition (D_C^*=weir opening gap/diameter =0.196), air pocket entrapment was observed at three upstream pressure values. When the downstream weir opening value was further increased, at 0.027 m (value of weir opening = 0.027 m, Dc*=weir opening/Diameter =0.263, air pocket formation was observed at an upstream pressure of 0.61 m and 0.915 m, but no air pocket formation was observed at a pressure of 0.305 m. This result shows that for higher upstream pressure heads and pipe filling flow rates air pocket entrapment was prevalent. Similarly, at the value of 0.020 m weir opening, the smallest weir opening value studied in this study, air pocket entrapment was observed for all upstream pressure head conditions. Also, no air pocket entrapment was observed for any pressure condition in the case of a fully open weir opening. The results for air pocket entrapment conditions were consistent with the SFI threshold criterion presented by Li and McCorquodale (1999). The agreement with the modified criteria based on Kordyban (1990) was not so good, and based on this study it probably should not be used in the context of SFI prediction, despite of its greater simplicity.

It was determined that multiple air pocket entrapment can occur during the propagation of the pressurization interface in a single pipe reach. The location of the pressurization interface migrated ahead of the initial pipe filling bore as a pocket was entrapped, which was an interesting result that confirmed the observation by Li and McCorquodale (1999). If this occurs multiple times, the spread of pressurized conditions in the pipe will be further accelerated. It is speculated that these multiple pockets can be linked with sequence of geysering events that are observed in stormwater systems. In addition, experiments showed that the trapped air pockets may merge during the rapid filling process.

Experimental observations of air pockets dimensions as well associated scale effects in the entrapment process are still unanswered questions. Experimental systems can be performed in the

future by changing the dimensional proportions and the geometry of the pipe, particularly the pipe diameter. Furthermore, apparatuses may be improved in the future and enable direct measurement of entrapped air pocket thickness and related pocket volume. Future experiments can also evaluate the effects of entrapped air pockets in conditions of varying slope leading to varying propagation velocity of pressurization fronts. Finally, further numerical modeling studies with CFD can be developed, possibly with improved representation of turbulence modeling and of boundary conditions.

Bibliography

Baines, B. W. D. (1991). Air Cavities as Gravity Currents on Slope. *Journal of Hydraulic Engineering, ASCE, 117*(12), 1600–1615. https://doi.org/10.1061/(ASCE)0733 9429 (1991)117:12(1600)

Baines, P. G., and Mitsudera, H. (1994). On the mechanism of shear flow instabilities. *Journal of Fluid Mechanics, 276*(1), 327. https://doi.org/10.1017/S0022112094002582

Batchelor, G.K. (1967). *An introduction to the fluid dynamics*. Cambridge University Press. Cambridge, UK

Benjamin, T. B. (1968). Gravity currents and related phenomena. *Journal of Fluid Mechanics, 31*(02), 209–248. https://doi.org/10.1017/S0022112068000133

Chanson, H. (1996). Air Bubble Entrainment in Free-Surface Turbulent Shear Flows. Academic Press. London, U. K.

Chosie, C. D., Hatcher, T. M., and Vasconcelos, J. G. (2014). Experimental and Numerical Investigation on the Motion of Discrete Air Pockets in Pressurized Water Flows. *Journal of Hydraulic Engineering, 140(*8), 04014038. https://doi.org/10.1061/(ASCE)HY.1943. 7900.0000898

Gardner, G.C. and Crow, I.G. (1970). The motion of large bubbles in horizontal channels. *Journal of Fluid Mechanics, 43*: 247–255, 1970.

Granata, F., de Marinis, G., and Gargano, R. (2014). “Flow-improving elements in circular drop

manholes.” *Journal of Hydraulic Research*, Taylor & Francis, 52(3), 347–355.

Gualtieri, C., and Chanson, H. (2013). “Interparticle arrival time analysis of bubble distributions in a dropshaft and hydraulic jump.” *Journal of Hydraulic Research*, 51(3), 253–264.

Hamam, M.A. and McCorquodale, A. (1982). Transient conditions in the transition from gravity to surcharged sewer flow. *Canadian Journal Civil Engineering*, (9): 189–196, 1982.

Kordyban, E. (1990). Horizontal slug flow: a comparison of existing theories. *Journal of Fluids Engineering, 112*(3), 1–10. https://doi.org/10.1115/1.2909372

Lauchlan, C.S., Escarameia, M., May, R.W.P., Burrows, R. and Gahan, C.(2005). Air in pipelines - A literature review. HR *Wallingford Technical Report SR.*, 649.

Lautenbach, D. J., Vasconcelos, J. G., Wright, S. J., Wolfe, J. R., Cassidy, J. F. and Klaver, P. R. (2008). Analysis of transient surge in the proposed District of Columbia Water and Sewer Authority deep tunnel system. *Proc., 2008 WEF Collection Systems Conference, Pittsburgh*, PA., 2008.

Lewis, J.W. and Wright, S.J. (2012). Air-Water Interactions that Generate Large Water Lift through Vertical Shafts in Stormwater Conduits. *Jòurnal of Water Management Modeling*, DOI: 10.14796/JWMM.R245-02, 2012.

Li, J. and, McCorquodale, A. (1999). Modeling Mixed Flow in Storm Sewers. *Journal of Hydraulic Engineering*, 125(1983), 1170–1180..

Ma, Y., Zhu, D. and Rajaratnam, N., (2016). Air Entrainment in a Tall Plunging Flow Dropshaft Air Entrainment in a Tall Plunging Flow Dropshaft. *Journal of Hydraulic Engineering* DOI:10.1061/(ASCE)HY.1943-7900.0001181, 2016.

Martin, C.S. (1976). Entrapped air in pipelines. *Proc., 2nd International Conference on Pressure Surges, BHR, Bedford, England*, 15–28, 1976.

Muller, K. Z., Wang, J., and Vasconcelos, J. G. (2017). Water Displacement in Shafts and Geysering Created by Uncontrolled Air Pocket Releases. *Journal of Hydraulic Engineering, 143*(10), 1–13. https://doi.org/10.1061/(ASCE)HY.1943-7900.0001362.

Patrick, A. and Vasconcelos, J. G. (2015). Air Entrainment Effects on the Pressure Wave Celerities Following Rapid Filling Pipe Flows. *Proc. 2015 ASCE EWRI Congress,* Austin, TX. pp. 1638-1647. DOI: 10.1061/9780784479162.159

Rajaratnam, N., Mainali, A., and Hsung, C. Y. (1997). "Observations on Flow in Vertical Dropshafts in Urban Drainage Systems." *Journal of Environmental Engineering*, 123(5), 486–491.

Ramezani, L., M., Karney, B. and Malekpour, A., (2016). "Encouraging Effective Air Management in Water Pipelines : A Critical Review. *Journal of Hydraulic Engineering,* DOI: 10.1061/ (ASCE)WR.1943-5452.0000695,2016.

Simpson, J.E. (1997). Gravity currents in the environment and the laboratory. Cambridge University Press, 1997.

Townson, D. (1991). *Free-Surface Hydraulics*. London: CRC Press.

Vasconcelos, J. G. and Wright, S. J. (2006a). Mechanisms for Air Pocket Entrapment in Stormwater Storage Tunnels. *Proc. World Environmental and Water Resources Congress 2006, 40856*(1999), 9–9. https://doi.org/10.1061/40856(200)9.

Vasconcelos,J.G. and Wright, S. (2008). Rapid Flow Startup in Filled Horizontal Pipelines. *Journal of Hydraulic Engineering, 134(7),* 1094–1100. https://doi.org/10.1061/(ASCE)0733-9429(2008)134

Vasconcelos, J.G. and Wright, S.J. (2011). Geysering generated by large air pockets released through water-filled ventilation shafts. *Journal of Hydraulic Engineering., 135*(5): 543–555,

2011.

Vasconcelos, J.G. and Leite, G.M. (2012). Pressure surges following sudden air pocket entrapment in stormwater tunnels. *Journal of Hydraulic Engineering, 138*(12): 1080–1089, 2012.

Wilkinson, D.L. (1982). Motion of air cavities in long horizontal ducts. *Journal of Fluid Mechanics.*, 118: 109–122, 1982.

Wylie, E. and Streeter, V. (1993). *Fluid transients in systems*. Prentice Hall, Upper Saddle River, NJ.

Zhou, F., Hicks, F.E. and Steffler, P.M. (2002). Transient flow in a rapidly filling horizontal pipe containing trapped air. *Journal of Hydraulic Engineering, 128*(6): 625–634, 2002.